

ITP-SB-98-28
BNL-HET-98/17

Single Transverse-Spin Asymmetries in Hadronic Pion Production

Jianwei Qiu^{1*} and George Sterman²

¹*Physics Department, Brookhaven National Laboratory
Upton, New York 11973-5000, USA*

²*Institute for Theoretical Physics, State University of New York
Stony Brook, New York 11794-3840, USA*

(June 4, 1998)

Abstract

We analyze single transverse-spin asymmetries for hadronic pion production at large transverse momenta using QCD factorization. In the large x_F region, leading contributions to the asymmetries are naturally produced by twist-3 parton correlation functions that couple quark fields and gluon field strengths. With a simple model for these matrix elements, leading-order asymmetries calculated from QCD are consistent with data on pion production from Fermilab, and can be used to predict single-spin asymmetries at RHIC. We argue that our perturbative calculation for the asymmetries is relevant to pion transverse momenta as low as a few GeV.

PACS: 12.38Bx, 13.85.-t, 13.85.Ni, 13.88.+e

*On-leave from Department of Physics and Astronomy, Iowa State University, Ames, Iowa 50011, USA.

I. INTRODUCTION

Perturbative Quantum Chromodynamics (QCD) has been successful in interpreting and predicting spin-averaged scattering cross sections at large momentum transfer. Since quarks and gluons carry spin, we expect QCD to apply to hard spin-dependent scattering as well. However, high energy experiments with polarized beam and/or target have provided many theoretical challenges. For example, data on the spin asymmetries in deep-inelastic scattering (DIS) of polarized leptons on polarized hadrons [1] sparked a wave of theoretical effort in understanding the nature of the nucleon's spin [2].

A spin asymmetry is the difference of two polarized cross sections, with opposite directions of polarization, divided by their sum. Asymmetries can be obtained with both beams (or beam and target) polarized or only one beam (or target) polarized. The former is a double spin asymmetry, and the latter a single spin asymmetry. Depending on the direction of the polarization, we can have longitudinal-spin asymmetries, if the polarization is along the beam direction, and/or transverse-spin asymmetries, when the spin is polarized perpendicular to the beam direction.

Because of parity and time-reversal invariance, single longitudinal-spin asymmetries for single-particle inclusive production vanish for the strong interactions. However, experimentally-significant single transverse-spin asymmetries have been observed in Λ production, as well as pion production, for almost twenty years [3,4]. These single transverse-spin asymmetries are of the order of ten or more percent of the unpolarized cross section. Experimental results on pion production have been very consistent, and the effects persist to pion transverse momenta of several GeV, into the hard-scattering region, where perturbative QCD (pQCD) has had success in describing spin-averaged cross sections [5]. The extension of the pQCD formalism to spin-dependent cross sections, however, has not been completely straightforward. It was pointed out long ago [6] that QCD perturbation theory predicts vanishing single transverse-spin asymmetries at high p_T . Efremov and Teryaev later pointed out that a nonvanishing single transverse-spin asymmetry can be obtained in pQCD if one goes beyond the leading power [7,8]. However, the relatively large size and peaking in the forward direction of observed effects remained a difficulty [9].

Some time ago, using the example of hadronic direct photon production [10], we demonstrated that single transverse-spin asymmetries can be consistently evaluated in terms of generalized factorization theorems in perturbative QCD [11]. The asymmetries are presented as a sum of terms, each of which consists of a convolution of a twist-2 parton distribution from the unpolarized hadron, a twist-3 quark-gluon correlation function from the polarized hadron, and a short-distance partonic hard part calculable in perturbative QCD. The twist-3 quark-gluon correlation functions reflect the interaction of quarks with the color field of the hadron [10,12,13]. In order to test this formalism, we need to have more than one physical process to extract information on these new and fundamental correlation functions, and to test their universality. Recent work has explored their role in the Drell-Yan process [14]. In this paper, we will not explore the physical interpretation of the correlation functions beyond what is currently in the literature. Rather, we concentrate on the extension of the formalism to pion production.

In the forward region for pion production, where x_F is large, we shall argue that leading contributions to the asymmetry depend on only one twist-3 matrix element (given in Eq.

(25) below), which couples two quark fields and one gluon field strength. This is the same matrix element that gives the leading contribution to single transverse-spin asymmetries in direct photon production [10]. With a simple model for this twist-3 matrix element, we show that significant asymmetries can be generated, and that the asymmetries increase naturally as a function of x_F . Our simple model has two parameters: one for the normalization, and the other for the relative sign between the up and down quark correlation functions. Extrapolating from measured single transverse-spin asymmetries in π^+ and π^- production in proton(\uparrow)-proton collisions [4], we fix these two parameters in our model. We can then derive both the sign and shape of the asymmetries for π^0 production, as well as pion production in collisions with a polarized antiproton beam. Our results are consistent with data from Fermilab experiments. The model then predicts the normalization, x_F and transverse-momentum dependence of the asymmetries at higher energies. These predictions can be tested at RHIC.

The naive expectation for the twist-3 asymmetry, A_N , is λ/ℓ_T , with λ a nonperturbative scale from the twist-3 matrix element and ℓ_T the transverse momentum of the observed particle. A pure $1/\ell_T$ dependence, however, decreases quickly as ℓ_T increases, and becomes ill-defined when ℓ_T is small. Consequently, one might worry that the range of ℓ_T where the asymmetry is not too small, while ℓ_T is large enough to use pQCD, is very limited, and that the region to study twist-3 physics might be too limited to be interesting. In fact, we shall see below that single transverse-spin asymmetries are a very good observable to study twist-3 physics perturbatively.

In contrast to the naive expectation, for the kinematics of the Fermilab data, the λ/ℓ_T contribution to A_N is not the dominant source of the asymmetry. From dimensional analysis alone, the asymmetry A_N admits two types of contributions, which are proportional to $\lambda\ell_T/(-U)$ as well as $\lambda\ell_T/(-T) \sim \lambda/\ell_T$, with U and T Mandelstam variables. Their relative contributions can be determined by perturbative calculation. For large x_F , where the asymmetry is large experimentally, U is larger than T , but we shall show in this paper that the coefficient for the $\lambda\ell_T/(-U)$ term is much larger than that of the λ/ℓ_T term in this region (see Eq. (76)). As we will see in Sec. V, the transverse momentum dependence of the asymmetry is actually quite mild for ℓ_T from less than 2 up to 6 GeV at $x_F = 0.4$, where much of the Fermilab data were collected. This conclusion is very encouraging for future applications of perturbative QCD beyond the level of leading twist.

Our method and results can be generalized to single transverse-spin asymmetries in other single particle production. With the extracted information on twist-3 matrix elements, we can predict both the sign and magnitude of single transverse-spin asymmetries for any inclusive single-particle production, such as for direct photons, kaons, or other hadrons.

Related work on single-spin asymmetries involves the incorporation of parton transverse momenta, either in parton distributions [15,16] or fragmentation functions [17–19]. There is considerable evidence that at transverse momenta in the range of a few GeV, “ k_T -smearing” effects can be important [5,20] in spin-averaged cross sections. It would seem natural to include them in the same range for single-spin asymmetries as well. Whether they should be thought of as the dynamical source of the asymmetry remains to be seen. The fragmentation analysis requires the introduction of “chiral-odd” distribution functions [17,19], which combine with the leading-twist transversity function [21,22] to produce nonvanishing asymmetries. We shall discuss how these effects can arise in the context of twist-3 factor-

ization theorems, but our explicit models will be based for simplicity on chiral-even parton distributions only.

The twist-three analysis described here is in some sense a minimalist approach, depending on only light-cone variables, which we hope can serve as a benchmark for models which include models of both light-cone and transverse degrees of freedom. Other descriptions of single-spin asymmetries are based on multiquark interactions [23] and orbital motion [24]. Interesting comparisons of different approaches may be found in [25] and [26].

Our paper is organized as follows. In Sec. II, we define single transverse-spin asymmetries in single particle production in hadronic collisions. We introduce generalized factorization formulas for the asymmetries, identify terms that we expect to dominate in the large- x_F region, review the factorization procedure at twist-three and leading order, and recall the leading-order spin-averaged cross sections to which we compare. In Sec. III, we present our explicit calculations of single transverse-spin asymmetries in hadronic pion production. We express these asymmetries in terms of short-distance partonic cross sections (coefficient functions), calculated in perturbative QCD, and non-perturbative twist-3 matrix elements. Using a simple model for the twist-3 matrix elements, we compare our calculated asymmetries with experimental data in Sec. IV. Finally, in Sec. V, we give a summary of our results, and an outlook for the subject. We have also included an appendix, in which we review the application of parity and time reversal symmetry, and identify the list of chiral-even and chiral-odd twist-3 distributions and fragmentation functions that can contribute to the single-spin asymmetry for pion production.

II. SINGLE TRANSVERSE-SPIN ASYMMETRIES

A. Definition and General Considerations

Single spin asymmetries are introduced for reactions in which only one particle is polarized. For example, consider single-particle inclusive production in a high energy collision,

$$A(P, \vec{s}) + B(P') \longrightarrow C(\ell) + X , \quad (1)$$

where A and B are the initial particles, with A polarized, where C is the observed particle (say, a pion) of momentum ℓ , and where X represents all other particles in the final state. In order to fix the kinematics, we choose the center of mass frame of the incoming hadrons, with the z -axis along the momentum of the polarized hadron. We introduce two four-vectors, \bar{n}^μ and n^μ ,

$$\begin{aligned} \bar{n}^\mu &\equiv (\bar{n}^+, \bar{n}^-, \bar{n}_T) \equiv (1, 0, 0_T) , \\ n^\mu &\equiv (0, 1, 0_T) , \end{aligned} \quad (2)$$

with $\bar{n}^2 = 0 = n^2$, and $\bar{n} \cdot n = 1$. The incoming hadrons' momenta are $P^\mu \sim \bar{n}^\mu \sqrt{S/2}$, and $P'^\mu \sim n^\mu \sqrt{S/2}$, respectively. Invariants at the hadron level are defined as

$$\begin{aligned} S &= (P + P')^2 \approx 2P \cdot P' \\ T &= (P - \ell)^2 \approx -2P \cdot \ell \\ U &= (P' - \ell)^2 \approx -2P' \cdot \ell , \end{aligned} \quad (3)$$

where hadron masses are neglected. Given Eq. (3), we next introduce

$$x_F = \frac{2\ell_z}{\sqrt{S}} = \frac{T - U}{S} ,$$

$$x_T = \frac{2\ell_T}{\sqrt{S}} . \quad (4)$$

We now introduce $\sigma(\ell, \vec{s})$ as the cross section of the process given in Eq. (1). The spin-averaged cross section for single-particle inclusive production may be represented as

$$\sigma(\ell) \equiv \frac{1}{2} [\sigma(\ell, \vec{s}) + \sigma(\ell, -\vec{s})] , \quad (5)$$

and the corresponding spin-dependent cross section as

$$\Delta\sigma(\ell, \vec{s}) \equiv \frac{1}{2} [\sigma(\ell, \vec{s}) - \sigma(\ell, -\vec{s})] . \quad (6)$$

The single spin asymmetry is often defined as a dimensionless ratio of spin-dependent and spin-averaged cross sections,

$$A(\ell, \vec{s}) \equiv \frac{\Delta\sigma(\ell, \vec{s})}{\sigma(\ell)} = \frac{\sigma(\ell, \vec{s}) - \sigma(\ell, -\vec{s})}{\sigma(\ell, \vec{s}) + \sigma(\ell, -\vec{s})} . \quad (7)$$

A single longitudinal-spin asymmetry is denoted as A_L , and a single transverse-spin asymmetry as A_N . We shall be concerned in this paper with A_N . For differential cross sections, the asymmetry can be defined as

$$A_N(\ell, s_T) = \frac{E_\ell d^3\Delta\sigma(\ell, \vec{s}_T)/d^3\ell}{E_\ell d^3\sigma(\ell)/d^3\ell} , \quad (8)$$

where $E_\ell d^3\sigma/d^3\ell$ and $E_\ell d^3\Delta\sigma/d^3\ell$ are the Lorentz invariant spin-averaged and spin-dependent cross section, respectively. In this paper, we will concentrate on single transverse-spin asymmetries in the forward region (i.e., large x_F) where the asymmetries are largest [4].

Due to the symmetries of fundamental interactions, it is possible to have a vanishing single transverse-spin asymmetry, even though the corresponding total cross section $\sigma(\ell, \vec{s})$ itself is finite. For example, it was pointed out by Christ and Lee over 30 years ago [27] that time-reversal invariance forbids single transverse-spin asymmetries in inclusive deep-inelastic scattering (DIS) to lowest order in α_{EM} . Let us review the reason.

Consider a general inclusive lepton-hadron deep-inelastic scattering, which is the analog of Eq. (1),

$$L(\ell) + H(P, \vec{s}_T) \longrightarrow L(\ell') + X , \quad (9)$$

where $L(\ell)$ and $L(\ell')$ are unpolarized incoming and outgoing leptons of momenta, ℓ and ℓ' , respectively, and $H(P, \vec{s}_T)$ represents the polarized target hadron with its spin \vec{s}_T perpendicular to the beam momentum. In the approximation of one-photon exchange, as shown in Fig. 1, the inclusive cross section $\sigma(\vec{s}_T)$ can be expressed as

$$\sigma(\vec{s}_T) \propto L^{\mu\nu} W_{\mu\nu}(\vec{s}_T) , \quad (10)$$

where the leptonic tensor, $L^{\mu\nu}$, is symmetric, and the hadronic tensor is given in terms of matrix elements of electromagnetic currents,

$$W_{\mu\nu}(\vec{s}_T) \propto \langle P, \vec{s}_T | j_\mu^\dagger(0) j_\nu(y) | P, \vec{s}_T \rangle . \quad (11)$$

Applying parity and time-reversal (PT) and translation invariance to the matrix element in Eq. (11), we obtain following relation,

$$\langle P, \vec{s}_T | j_\mu^\dagger(0) j_\nu(y) | P, \vec{s}_T \rangle = \langle P, -\vec{s}_T | j_\nu^\dagger(0) j_\mu(y) | P, -\vec{s}_T \rangle . \quad (12)$$

Combining Eqs. (11) and (12), we find

$$W_{\mu\nu}(\vec{s}_T) = W_{\nu\mu}(-\vec{s}_T) . \quad (13)$$

From Eq. (6), we obtain the spin-dependent cross section for inclusive deep-inelastic scattering,

$$\begin{aligned} \Delta\sigma(\vec{s}_T) &\propto L^{\mu\nu} [W_{\mu\nu}(\vec{s}_T) - W_{\mu\nu}(-\vec{s}_T)] \\ &= L^{\mu\nu} [W_{\mu\nu}(\vec{s}_T) - W_{\nu\mu}(\vec{s}_T)] \\ &= 0 , \end{aligned} \quad (14)$$

where in the second line we use Eq. (13) and in the third the symmetry of $L^{\mu\nu}$ when the lepton is unpolarized. From Eqs. (7) and (14), it is clear that the single transverse-spin asymmetry for inclusive deep-inelastic scattering, A_N^{DIS} , vanishes to lowest order in α_{EM} .

In hadron-hadron scattering, in contrast, the presence of multiple (initial-state or final-state) interactions prevents a simple decomposition like Eq. (10), and allows single transverse-spin asymmetries for final-state photons as well as hadrons [8,10]. Experimentally, data from Fermilab show large single transverse-spin asymmetries in single pion production [4], and at the same time, show no apparent single transverse-spin asymmetries in prompt photon production in the central (low x_F) region [28].

Experiments at Fermilab for pion (π^\pm, π^0) and prompt photon production were carried out with a 200 GeV polarized proton (or antiproton) beam on an unpolarized proton target. The observed single transverse-spin asymmetries of inclusive single pion production can be as large as 20 to 30% in the forward region. In addition to the large values of the asymmetries, a number of other interesting features are evident in the data. For example, a strong rise of the asymmetries with x_F was observed for all pion charges. When the beam was switched from polarized proton to polarized antiproton, the same sign of the asymmetry was observed for π^0 , while the sign of the asymmetry for π^+ , as well as π^- , changed. Both beams had opposite signs of the asymmetries of π^+ and π^- .

Perturbative QCD was first used to study the effects of single transverse-spin asymmetries by Kane, Pumplin, and Repko (KPR) [6]. KPR calculated the single transverse-spin asymmetry for single hadron (pion) production in terms of a QCD parton model. By calculating the quark-quark scattering diagrams shown in Fig. 2, KPR found that the nonvanishing single transverse-spin asymmetry for large- p_T reactions is proportional to the quark mass: $A_N \propto T_m \sim m_q \langle P, \vec{s}_T | \bar{\psi} \Gamma \psi | P, \vec{s}_T \rangle$, where, for example, $\Gamma = \gamma^+ \gamma_5 \gamma_T$. Consequently,

the asymmetry vanishes in the scaling limit ($m_q \rightarrow 0$). Although this calculation does not explain the observed large single transverse-spin asymmetries [6,7], the fact that the result is proportional to the quark mass indicates that the single transverse-spin asymmetry is a twist-3 effect in QCD perturbation theory [8,10,29].

QCD dynamics, however, is much richer than the parton model. In addition to the parton mass effects just discussed, there are other twist-3 contributions. Because quarks are not exactly parallel to the incoming hadron beam, twist-3 contributions also arise from “intrinsic” transverse momentum, which is proportional to $T_{k_T} \sim \langle P, \vec{s}_T | \bar{\psi} \Gamma \partial_T \psi | P, \vec{s}_T \rangle$. In addition, there are twist-3 contributions from the interference between a quark state and a quark-gluon state, which is proportional to $T_{A_T} \sim \langle P, \vec{s}_T | \bar{\psi} \Gamma A_T \psi | P, \vec{s}_T \rangle$. Due to gauge invariance, T_{k_T} and T_{A_T} are not independent, and can be combined to form $T_{D_T} \sim \langle P, \vec{s}_T | \bar{\psi} \Gamma D_T \psi | P, \vec{s}_T \rangle$, and/or $T_F \sim \langle P, \vec{s}_T | \bar{\psi} \Gamma F^+_T \psi | P, \vec{s}_T \rangle$, with $F^+_T \propto [D^+, D_T]$, where D_μ is the covariant derivative. Therefore, in addition to parton mass effects, single transverse-spin asymmetries can be proportional to the twist-3 matrix elements T_{D_T} and T_F [8,10,29]. These twist-3 matrix elements involve three field operators ($\bar{\psi} \Gamma D_T \psi$, $\bar{\psi} \Gamma F^+_T \psi$, or with the quark fields replaced by gluon field strengths [30]). Also, different choices for the Dirac matrices Γ in the operators give different twist-3 matrix elements (see the Appendix) [10].

Because of their odd numbers of field operators, three-field twist-3 matrix elements do not have the probability interpretation of parton distributions, which are proportional to matrix elements of twist-2 operators, $\bar{\psi} \Gamma \psi$ or $F^+_T F^+_T$. In principle, however, they are as fundamental as the parton distributions. Measurements of twist-3 distributions, or three-field correlation functions, provide us new opportunities to study QCD dynamics.

B. Factorization and the Valence Quark Approximation

As we have seen, spin-dependent asymmetries for hadronic pion production with one hadron transversely polarized vanish at large momentum transfer [6]. Nonvanishing values of the single transverse-spin asymmetry signal non-leading power contributions. According to the basic factorization theorems [31], the leading power spin-averaged cross section for the production of a pion with large transverse momentum ℓ_T can be factorized into *four* separated functions, as sketched in Fig. 3,

$$\sigma_{A+B \rightarrow \pi} = \sum_{abc} \phi_{a/A}(x) \otimes \phi_{b/B}(x') \otimes \hat{\sigma}_{a+b \rightarrow c} \otimes D_{c \rightarrow \pi}(z) , \quad (15)$$

where \sum_{abc} represents the sum over parton flavors: quark, antiquark and gluon. In Eq. (15), $\phi_{a/A}(x)$ and $\phi_{b/B}(x')$ are probability densities to find parton a of momentum xP in hadron A and parton b of momentum $x'P'$ in hadron B , respectively. As noted above, they may be interpreted in terms of expectation values in the hadronic state of two-field matrix elements, for example $\bar{\psi} \Gamma \psi$ or $F^+_T F^+_T$. $D_{c \rightarrow \pi}(z)$ is the fragmentation function for a parton c of momentum $p_c = \ell/z$ to fragment into a pion of momentum ℓ , and $\hat{\sigma}_{a+b \rightarrow c}$ is a short-distance partonic part (the Born cross section plus corrections), calculable perturbatively order-by-order in α_s . The symbol \otimes in Eq. (15) represents the convolution over the corresponding parton momentum fraction. In terms of the Lorentz invariant differential cross section, Eq. (15) can be written as [5]

$$E_\ell \frac{d^3\sigma_{A+B \rightarrow \pi}}{d^3\ell} = \sum_{abc} \int dx \phi_{a/A}(x) \int dx' \phi_{b/B}(x') \int \frac{dz}{z} \left(E_c \frac{d^3\hat{\sigma}_{a+b \rightarrow c}}{d^3p_c} \right) \frac{D_{c \rightarrow \pi}(z)}{z} . \quad (16)$$

The predictive power of Eq. (16) depends on independent measurements of the non-perturbative functions, $\phi_{a/A}$, $\phi_{b/B}$ and $D_{c \rightarrow \pi}$, and the calculation of the partonic part $E_c d^3\hat{\sigma}_{a+b \rightarrow c}/d^3p_c$.

Just as for most other physical observables calculated in perturbative QCD, the predictive power of the theory for twist three relies on factorization theorems [31]. Physical observables that depend on the transverse polarization of a single hadron are typically power corrections to the total cross section, in comparison with spin-averaged or longitudinally polarized cross sections. In Ref. [32], for a physical observable with a large momentum transfer Q , we extended the factorization program to $O(1/Q^2)$ corrections for unpolarized hadron-hadron cross sections, and in [11,33] to $O(1/Q)$ corrections in polarized cross sections.

Following the generalized factorization theorem [11,33], the transverse spin-dependent cross section for large ℓ_T pions, $\Delta\sigma(\vec{s}_T)$, can be written in much the same way as the spin-averaged cross section, Eq. (15), as a sum of three generic higher-twist contributions, each of which can also be factorized into four functions,

$$\begin{aligned} \Delta\sigma_{A+B \rightarrow \pi}(\vec{s}_T) = & \sum_{abc} \phi_{a/A}^{(3)}(x_1, x_2, \vec{s}_T) \otimes \phi_{b/B}(x') \otimes H_{a+b \rightarrow c}(\vec{s}_T) \otimes D_{c \rightarrow \pi}(z) \\ & + \sum_{abc} \delta q_{a/A}^{(2)}(x, \vec{s}_T) \otimes \phi_{b/B}^{(3)}(x'_1, x'_2) \otimes H''_{a+b \rightarrow c}(\vec{s}_T) \otimes D_{c \rightarrow \pi}(z) \\ & + \sum_{abc} \delta q_{a/A}^{(2)}(x, \vec{s}_T) \otimes \phi_{b/B}(x') \otimes H'_{a+b \rightarrow c}(\vec{s}_T) \otimes D_{c \rightarrow \pi}^{(3)}(z_1, z_2) \\ & + \text{higher power corrections} , \end{aligned} \quad (17)$$

where \sum_{abc} represents sums over parton flavors: quark, antiquark and gluon, and where $\phi_{b/B}(x')$ and $D_{c \rightarrow \pi}(z)$ are standard twist-two parton distributions and fragmentation functions, respectively. In Eq. (17), the first term corresponds to the process sketched in Fig. 4a, and the second and third terms correspond to the ones sketched in Fig. 4b.

For the first term in Eq. (17), nonvanishing contributions to $\Delta\sigma(\vec{s}_T)$ come from twist-3 parton distributions (correlation functions) $\phi_{a/A}^{(3)}(x_1, x_2, \vec{s}_T)$ in the polarized hadron. For the second and third terms, the contributions to $\Delta\sigma(\vec{s}_T)$ involve the twist-2 transversity distributions $\delta q_{a/A}^{(2)}(x, \vec{s}_T)$ [21,22]. Because the operator in the transversity distribution requires an even number of γ -matrices [21,22], the second term and third terms in Eq. (17) also include a twist-3, chiral-odd parton distribution $\phi_{b/B}^{(3)}(x'_1, x'_2)$ from the unpolarized hadron B , or a twist-3, chiral-odd fragmentation function, $D_{c \rightarrow \pi}^{(3)}(z_1, z_2)$. In the factorized form of Eq. (17), PT invariance may be applied in a manner analogous to the treatment of the DIS cross section given above. In this case, however, PT invariance allows nonzero A_N for a limited number of functions, as discussed in the Appendix.

As in the spin-averaged cross section, Eq. (15), the hard-scattering functions $H_{a+b \rightarrow c}(\vec{s}_T)$ are the only factors in Eq. (17) that are calculable in QCD perturbation theory. The calculation of the H 's depends on the explicit definitions of the twist-3 distributions, for example $\phi_{a/A}^{(3)}(x_1, x_2, \vec{s}_T)$, and the predictive power of Eq. (17) relies on the universality of the new twist-3 distributions [11,33].

Eq. (17) illustrates the typical complexity of higher-twist analysis: even at first nonleading twist, whole new classes of functions begin to contribute. This complexity is particularly difficult to sort out for physical observables to which leading-twist terms contribute. The combination of small effects and complex parameterizations has made the extraction of higher twist distributions from the data difficult, despite the considerable effort that has been invested in the formalism [34,35].¹ The vanishing of single-spin asymmetries at leading power solves one of these problems, the masking of higher twist by leading twist. Beyond this, however, it is clear that to fully disentangle all of the functions contributing to Eq. (17) would require a constellation of data and a level of analysis far beyond what is currently available. Turning specifically to the first term in Eq. (17), we observe that the index a refers to pairs of partons, and that the functions $\phi_{a/A}^{(3)}$ are correspondingly functions of two momentum fractions. In addition, even assuming that we knew this set of functions, we would still be faced with the chiral-odd distributions and fragmentation functions in the second and third sums in Eq. (17). We would like to suggest, however, that by restricting ourselves to the limited kinematic range of large x_F for the observed particle, we may simplify the analysis greatly, and construct a simple model that explains the available data, and that provides extrapolations to higher energies and momentum transfers.

We are going to present a calculation of the large- x_F asymmetry at moderate or large ℓ_T , in terms of the chiral even functions $\phi_{a/A}^{(3)}(x_1, x_2, \vec{s}_T)$ only (first line of Eq. (17)). In these functions, we will consider only combinations of valence quark flavors with gluons. We will not find it necessary to specify these functions for all values of x_1 and x_2 , but only for the line $x_1 = x_2$, at which the gluon carries vanishingly small momentum fraction. We will refer to this set of simplifications as the *valence quark-soft gluon* approximation below. In this model, we thus neglect potential contributions from the transversity, coupled with the chiral-odd twist-3 distributions and fragmentation functions identified in the Appendix. We hope to explore these contributions elsewhere, but in the absence of independent information on the transversity, it seems natural to test the plausibility of a model based on chiral-even distributions alone.

First, consider our restriction to valence quarks. Given that single transverse-spin asymmetries were measured at Fermilab with a 200 GeV polarized beam [4], only partons (a and b in Eq. (16)) with large momentum fractions will be relevant for large x_F or ℓ_T . Because parton-to-pion fragmentation functions vanish as $z \rightarrow 1$, the effective momentum of the fragmenting parton, $p_c = \ell/z$, should be much larger than the pion momentum ℓ . Therefore, the dominant contribution to the cross sections in the central region should come from $x \sim x'$ in Eq. (17), with, in addition, x much larger than $x_T \approx 0.25$, which corresponds to $\ell_T \approx 4$ GeV at $E_{\text{beam}} = 200$ GeV. In our calculation we will concentrate on the forward region, where x_F is large. Similarly, in this region the dominant contributions to the cross section come from x considerably larger than x_T (i.e., $x > 0.25$) even for relatively small ℓ_T . For large x , there are few gluons or sea quarks from the beam hadron. Therefore, in our numerical calculations, we will keep only valence quarks from the polarized beam. That is, \sum_a in Eq. (17) now runs over only up and down valence quarks, coupled with a single gluon

¹We may note recent progress based on models of higher twist in deeply inelastic scattering and fragmentation inspired by renormalon analysis [36–38].

field.

In presenting this argument, we are well aware that in principle the flavor content of the twist three distributions may be totally different than those of twist two. Nevertheless, we consider it by far more natural to assume that three-field correlations at large x_i will be dominated by the same flavors as in the two-field, parton distribution, case. We recognize that this remains, however, an assumption. In our case, it means that we shall keep only valence quarks from the polarized beam, accompanied in twist-3 by gluons. In particular, we shall not consider three-gluon matrix elements [30].

We now turn to the question of “soft gluons”. To anticipate, the twist-three asymmetry involves only two classes of contributions in $H_{abc}(x_1, x_2)$. One of these is proportional to $\delta(x_1 - x_2)$, and the other to $\delta(x_i)$, $i = 1, 2$. The first case sets the momentum carried by the gluon field in the twist-3 matrix element into the hard scattering to zero, leaving the momenta carried by the two quark fields in the combination $\bar{\psi}F^{+T}\psi$ diagonal². In the second, one of the quark fields (ψ or $\bar{\psi}$) carries vanishing momenta. We refer to these two possibilities as “soft gluon” and “soft fermions” poles, respectively [10]. Soft gluon terms are typically accompanied by derivatives of the parton functions $\phi_{a/A}^{(3)}$, while soft fermion terms are not. We have emphasized in Ref. [10] that terms that involve derivatives with respect to distributions tend to be strongly enhanced near the edges of phase space, relative to those without derivatives. We shall see this in our explicit model below. We shall assume, in fact, that it is this effect that is primarily responsible for the experimentally-observed rise in single-spin asymmetries toward $x_F = 1$. We therefore suggest that only terms in which such derivatives occur need be kept, in order to describe the large- x_F single-spin asymmetry. In summary, only soft-gluon terms, from the first line of Eq. (17) produce the shape of the large asymmetries observed in the data in the forward region, and for these terms $x_1 = x_2$.

To set the stage for the explicit calculations of the next section, we first give an example of leading-order factorization at twist three for the spin-dependent cross section, following the method of Ref. [10]. This will enable us to trace the origin of twist-three spin distributions, and of the poles that underly the valence quark-soft gluon approximation that we have just described.

C. Twist-3 Factorization at Leading Order

The twist-3 correlation functions, $\phi_{a/A}^{(3)}(x_1, x_2, \vec{s}_T)$, depend on two parton momentum fractions, while twist-2 parton distributions, which are probability densities, depend on only one. Considering the effort and data needed to determine the parton distributions, it appears a difficult task to get a full description of these twist-3 distributions. From the general Feynman graphs contributing to the H ’s in Eq. (17), as shown in Fig. 5, it is also clear that there are many diagrams, even at lowest order. Their treatment is simplified, however, by taking advantage of the relation of the asymmetry to the pole structure of H [10]. This will enable us to evaluate $\Delta\sigma(\vec{s}_T)$ in Eq. (17) efficiently. Indeed, we will find that $\Delta\sigma(\vec{s}_T)$ depends on the twist-3 distributions through only a single independent momentum

²Note, there are no “soft gluons” in the short-distance functions H .

fraction, with the other fraction fixed by a pole. To see how this comes about, we consider a specific set of contributions, associated with the three classes of diagrams shown in Fig. 6. We first discuss the analysis of these diagrams according to the method of Ref. [10], and then briefly discuss other possibilities, reviewing why we expect those of Fig. 6 to dominate the asymmetry in the large- x_F region.

In our valence quark-soft gluon approximation, introduced in the last subsection, the fermion flavor a from the polarized hadron in Figs. 5 and 6 runs over valence quarks only, while parton b from the unpolarized hadron can be a gluon, valence quark or sea quark. We start from these three classes of diagrams, and derive below the factorized form for the spin-dependent cross section $\Delta\sigma(\vec{s}_T)$. The hard-scattering diagrams of Fig. 6 are all embedded in the overall process shown in Fig. 7a. The top part of this general diagram is proportional to the expectation value of an operator of the form $\bar{\psi}A_\sigma\psi$ in the polarized incoming hadron state $|P, \vec{s}_T\rangle$, while the bottom part includes the hard subprocess, as well as the target hadron matrix element and the final-state pion fragmentation function. In Fig. 7, k_1 and k_2 are valence quark momenta, and σ is the Lorentz index for the gluon field. We work, as in Ref. [10], in Feynman gauge. To derive a factorized expression for these contributions, we must separate spinor and color traces, as well as sums over vector Lorentz indices between the functions T and S .

After separation of all traces by a Fierz projection (see Appendix), the two functions T and S are connected only by the two momentum integrals that they share. The leading contributions of the general diagram shown in Fig. 7a can then be represented by the factorized diagrams shown in Fig. 7b, and can be written as

$$d\Delta\sigma(\vec{s}_T) \equiv \frac{1}{2S} \sum_a \int \frac{d^4k_1}{(2\pi)^4} \frac{d^4k_2}{(2\pi)^4} [T_a(k_1, k_2, \vec{s}_T) S_a(k_1, k_2)] , \quad (18)$$

where $1/2S$ is a flux factor, \sum_a runs over only valence flavors, $T_a(k_1, k_2, \vec{s}_T)$ is proportional to the matrix element of the operator, $(2\pi)[\bar{\psi}_a\gamma^+A^+\psi_a]/2P^{+2}$, and $S_a(k_1, k_2)$ represents the bottom part of the general diagram shown in Fig. 7b. The function $S_a(k_1, k_2)$ is contracted with $[(1/2)\gamma \cdot P P_\sigma] C_a/(2\pi)$, where the factor (2π) is due to the normalization of twist-3 matrix element T , which we will specify below. The color factor C_a is left from the factorization of color traces between $T_a(k_1, k_2, \vec{s}_T)$ and $S_a(k_1, k_2)$ [10]. With the function $T_a(k_1, k_2, \vec{s}_T) \propto \bar{\psi}A\psi$, the corresponding C_a is defined for all valence flavors a as

$$(C_a^B)_{ij} = \left(\frac{2}{N^2 - 1} \right) (t^B)_{ij} , \quad (19)$$

with $N = 3$ colors, B the gluon color index, and with quark color indices ij . The matrix $(t^B)_{ij}$ is the SU(3) generator in the defining representation of the group.

The next step in the factorization procedure is the “collinear” expansion [32,33], which will enable us to reduce the four-dimensional integrals in Eq. (18) to convolutions in the momentum fractions of partons, as in Eq. (17). Expanding S_a in the partonic momenta, k_1 and k_2 , around $k_1 = x_1 P$ and $k_2 = x_2 P$, respectively, we have

$$\begin{aligned} S_a(k_1, k_2) = S_a(x_1, x_2) &+ \frac{\partial S_a}{\partial k_1^\rho}(x_1, x_2) (k_1 - x_1 P)^\rho \\ &+ \frac{\partial S_a}{\partial k_2^\rho}(x_1, x_2) (k_2 - x_2 P)^\rho + \dots . \end{aligned} \quad (20)$$

This expansion, substituted in Eq. (18), allows us to integrate over three of the four components of each of the loop momenta k_i . The top part of the diagram T_a then becomes a twist-three light cone matrix element, convoluted with the terms of Eq. (20) in the remaining fractional momentum variables x_i .

As stressed in Refs. [8,10], some of the matrix elements that result from the collinear expansion can have nontrivial spin-dependence. It is at this stage that the pole structure of the hard scattering begins to play an important role. In fact, as shown in Refs. [8,10] and below, nonzero spin dependence is found *only* from pole terms in the hard scattering. Without these poles, the symmetries of the strong interaction force the asymmetry to vanish, in much the same fashion as for DIS above. Indeed, the poles provide exactly the sort of multiple interactions that are absent in DIS at lowest order in QED. The first term in the expansion, Eq. (20), $S_a(x_1, x_2)$, does not contribute to $\Delta\sigma(\vec{s}_T)$ when combined with $T_a(k_1, k_2, \vec{s}_T)$ in Eq. (18), because it lacks true initial- or final-state interactions. We will therefore drop it below.

Let us next look for poles in the diagrams of Fig. 6 from the remaining terms in Eq. (20), and identify the relevant twist-three matrix element. All of the diagrams in Fig. 6 provide a pole at $x_1 = x_2$ when $k_i = x_i P$ ($i = 1, 2$). As we will show below, these poles have the property that

$$\frac{\partial S_a}{\partial k_2^\rho}(x_1, x_2) = -\frac{\partial S_a}{\partial k_1^\rho}(x_1, x_2), \quad (21)$$

for $x_1 = x_2$. This equality is to be interpreted in the sense of distributions, since S_a is singular at $x_1 = x_2$. Substituting Eq. (21) into Eq. (20) and neglecting higher order derivatives, we have

$$S_a(k_1, k_2) \approx \frac{\partial S_a}{\partial k_2^\rho}(x_1, x_2) [\omega^{\rho\sigma}(k_2 - k_1)_\sigma], \quad (22)$$

where the projection operator $\omega^{\rho\sigma}$ is defined as $\omega^{\rho\sigma} \equiv g^{\rho\sigma} - \bar{n}^\rho n^\sigma$. Substituting Eq. (22) into Eq. (18) and performing the integration over the non-longitudinal components of the k 's, we derive

$$d\Delta\sigma(\vec{s}_T) = \frac{1}{2S} \sum_a \int dx_1 dx_2 \left[i\epsilon^{\rho s_T n \bar{n}} \frac{\partial S_a}{\partial k_2^\rho}(x_1, x_2) \right]_{k_2^\rho=0} T_{F_a}^{(V)}(x_1, x_2), \quad (23)$$

where the integration over x_1 (or x_2) will be fixed by the corresponding pole in $\partial S_a/\partial k_2$, and where $\epsilon^{\rho s_T n \bar{n}}$ is defined as

$$\epsilon^{\rho s_T n \bar{n}} = \epsilon^{\rho\sigma\mu\nu} \vec{s}_{T_\sigma} n_\mu \bar{n}_\nu. \quad (24)$$

The function $T_{F_a}^{(V)}(x_1, x_2)$ for flavor a in Eq. (23) is one of the twist-3 distributions introduced in Ref. [10],

$$\begin{aligned} T_{F_a}^{(V)}(x_1, x_2) &= \int \frac{dy_1^- dy_2^-}{4\pi} e^{ix_1 P^+ y_1^- + i(x_2 - x_1) P^+ y_2^-} \\ &\times \langle P, \vec{s}_T | \bar{\psi}_a(0) \gamma^+ \left[\epsilon^{s_T \sigma n \bar{n}} F_\sigma^+(y_2^-) \right] \psi_a(y_1^-) | P, \vec{s}_T \rangle. \end{aligned} \quad (25)$$

The ordered exponentials of the gauge field that make this matrix element gauge invariant have been suppressed [32,33]. It is easy to show that $T_{F_a}^{(V)}$ is real. Parity ensures that $T_{F_a}^{(V)} \sim \epsilon^{\rho n \bar{n} s}$, and time reversal invariance then implies that it is an even function of x_1 and x_2 ,

$$T_{F_a}^{(V)}(x_1, x_2) = T_{F_a}^{(V)}(x_2, x_1). \quad (26)$$

These properties are valuable in isolating nonvanishing asymmetries. For instance, the fact that $T_{F_a}^{(V)}$ is real ensures that only the poles of S in Eq. (23) can contribute.

Having factorized the twist-3 distribution $T_F^{(V)}$, we now factorize the remaining function $[i\epsilon^{\rho s t n \bar{n}} \partial S_a / \partial k_2]$ in Eq. (23) into a perturbatively calculable partonic part $H_{a+b \rightarrow c}$, a corresponding target parton distribution $\phi_{b/B}$ and a fragmentation function $D_{c \rightarrow \pi}$. At the leading power, diagrams contributing to $S_a(k_1, k_2)$ can be represented as in Fig. 8a, and can be factorized as

$$\begin{aligned} S_a(k_1, k_2) &\approx \sum_b \int \frac{d^4 k'}{(2\pi)^4} [M_{a+b}(k_1, k_2, k') B_b(k', P')] \\ &\approx \sum_b \int \frac{dx'}{x'} M_{a+b}(k_1, k_2, x') \phi_{b/B}(x'), \end{aligned} \quad (27)$$

where \sum_b runs over all parton flavors, and $\phi_{b/B}(x')$ is a twist-2 parton distribution for flavor b , for the unpolarized target hadron B . We use the matrix element definitions of twist-2 parton distributions given in Ref. [39]. Similarly, as shown in Fig. 8b, the factor $M_{a+b}(k_1, k_2, x')$ in Eq. (27) can be further factorized into a convolution of Feynman diagrams, calculable in perturbation theory, with standard twist-2 fragmentation functions,

$$M_{a+b}(k_1, k_2, x') \approx \sum_c \int dz H_{a+b \rightarrow c}(k_1, k_2, x', p_c = \ell/z) D_{c \rightarrow \pi}(z = \ell/p_c), \quad (28)$$

where the $H_{a+b \rightarrow c}$ are given by the diagrams of Fig. 6. The fragmentation functions $D_{c \rightarrow \pi}(z = \ell/p_c)$ are also defined as matrix elements in Ref. [39].

Finally, substituting Eq. (28) into Eq. (27), and Eq. (27) into Eq. (23), we derive a factorized expression for $\Delta\sigma(\vec{s}_T)$ in the form of Eq. (17),

$$\begin{aligned} d\Delta\sigma(\vec{s}_T) &= \frac{1}{2S} \sum_{abc} \int dz D_{c \rightarrow \pi}(z) \int \frac{dx'}{x'} \phi_{b/B}(x') \int dx_1 dx_2 T_{F_a}^{(V)}(x_1, x_2) \\ &\quad \times \left[i\epsilon^{\rho s t n \bar{n}} \frac{\partial}{\partial k_2^\rho} H_{a+b \rightarrow c}(k_1 = x_1 P, k_2 = x_2 P, x', p_c = \ell/z) \right]_{k_2^\rho=0}, \end{aligned} \quad (29)$$

where the integration over either x_1 or x_2 can be done by using the pole in $H_{a+b \rightarrow c}$. This results in a factorization with only a single momentum fraction for each of the incoming hadrons, similar to that for the spin-averaged cross section in Eq. (16), with $\phi_{a/A}(x)$ replaced by $T_{F_a}^{(V)}(x, x)$. In order to use this factorized formula for single transverse-spin asymmetries in pion production, in the following section we will evaluate the diagrams shown in Fig. 6 with off-shell momenta k_1 and k_2 . In each case, we will verify Eq. (21), or equivalently, observe that

$$\frac{\partial H}{\partial k_{2\rho}}(x_1, x_2 = x_1) = -\frac{\partial H}{\partial k_{1\rho}}(x_1, x_2 = x_1), \quad (30)$$

where, again, the equality is to be interpreted in terms of distributions.

D. Leading Contributions in the Forward Region

Before entering into the detailed calculations of the hard-scattering functions $H_{a+b \rightarrow c}$ in Eq. (29), we return to issue of why we believe that the dominant contribution is given by the $T_{F_a}^{(V)}$ in Eq. (29). We have already indicated that this is due to the derivative structure of these contributions. Let us see how these derivatives arise.

From the diagrams shown in Fig. 6, with the momenta p_c and $x'P'$ fixed, we get four typical sources of k_i ($i = 1, 2$) dependence: (1) k_i -dependence in $\delta(L(k_i)^2)$ with L the momentum of the unobserved final-state parton, (2) k_i -dependence in the propagators which go on-shell when $k_1 = k_2$, (3) k_i -dependence in the off-shell propagators, and (4) k_i -dependence in the numerators. The derivatives of $H_{a+b \rightarrow c}(k_1, k_2, x', p_c)$ with respective to k_i have the following features:

1. $(\partial/\partial k_i)\delta(L(k_i)^2)$ gives $\delta'(L(x_i P)^2)$, and its contribution to $\Delta\sigma(\vec{s}_T)$ is proportional to $(\partial/\partial x)T_F^{(V)}(x, x)$ after integration by parts;
2. $(\partial/\partial k_i)$ on a propagator that is potentially on-shell changes a single pole to a double pole, and the resulting integration over the double pole makes the contribution to $\Delta\sigma(\vec{s}_T)$ proportional to $(\partial/\partial x)T_F^{(V)}(x, x)$;
3. $(\partial/\partial k_i)$ on an off-shell propagator does not change the pole structure, and its contribution to $\Delta\sigma(\vec{s}_T)$ is proportional to $T_F^{(V)}(x, x)$ without a derivative;
4. $(\partial/\partial k_i)$ on k_i -dependence in the numerator gives contributions to $\Delta\sigma(\vec{s}_T)$ proportional to $T_F^{(V)}(x, x)$ without derivatives.

As we have pointed out earlier, we are interested in the asymmetries in the forward region, where x_F is large. Asymmetries in this region are dominated by large net momentum fraction x from the polarized beam parton, coupled with relatively small momentum fraction x' from the partons of the unpolarized target hadron. Since all distributions vanish as a power for large x , as $(1-x)^\beta$ with $\beta > 0$, $(\partial/\partial x)T_F^{(V)}(x, x) \gg T_F^{(V)}(x, x)$ when $x \rightarrow 1$. Therefore, in the forward region, terms proportional to derivative of the distributions $T_F^{(V)}$ dominate. In order to simplify our calculations of the largest effect, we keep only these terms. Thus, in Sec. III we will keep only those contributions corresponding to items (1) and (2) listed above.

Turning, finally, to other possible contributions in Eq. (17), we observe that it is only the matrix element $T_F^{(V)}$ that inherits derivative terms, as a result of the collinear expansion involving soft gluon poles. Soft fermion poles, of the sort discussed in Refs. [8,10] have no such derivatives at leading order. Soft-fermion poles also do not correspond to the valence quark approximation identified above, since they require one of the quark fields to carry zero momentum fraction. These features of the calculation follow exactly the same pattern as for direct photon production, as treated in Ref. [10], and we shall not repeat them here. It is only necessary to emphasize that the $T_F^{(V)}$ contributions from Fig. 6 are the complete set of derivative contributions at twist three and leading order, for the first (chiral even) term in Eq. (17).

E. Spin-Averaged Cross Sections for Hadronic Pion Production

In order to evaluate the asymmetries, defined in Eq. (8), we need to compute the leading-order spin-averaged cross section. QCD perturbation theory has been generally successful with experimental data on spin-averaged cross sections for inclusive single-pion production at large transverse momentum [5]. At leading order in α_s , only $2 \rightarrow 2$ Feynman diagrams, shown in Fig. 9, contribute to $E_c d^3 \hat{\sigma}_{a+b \rightarrow c} / d^3 p_c$. In terms of scattering amplitudes, the leading order $E_c d^3 \hat{\sigma}_{a+b \rightarrow c} / d^3 p_c$ can be expressed as [5]

$$E_c \frac{d\hat{\sigma}_{a+b \rightarrow c}}{d^3 p_c} = \frac{1}{16\pi^2 \hat{s}} \left| \overline{M}_{a+b \rightarrow c} \right|^2 \delta(\hat{s} + \hat{t} + \hat{u}) , \quad (31)$$

where \overline{M} is the spin-averaged amplitude. In Eq. (31), invariants at the parton level are given by

$$\begin{aligned} \hat{s} &= (xP + x'P')^2 = x x' S , \\ \hat{t} &= (xP - p_c)^2 = x T / z , \\ \hat{u} &= (x'P' - p_c)^2 = x' U / z , \end{aligned} \quad (32)$$

where S, T and U are defined in Eq. (3).

In the valence quark approximation, using the δ -function in Eq. (31) to fix the x' -integration in Eq. (16), we find the spin-averaged cross section for pion production at leading order in α_s ,

$$\begin{aligned} E_\ell \frac{d^3 \sigma}{d^3 \ell} &= \frac{\alpha_s^2}{S} \sum_{a,c} \int_{z_{\min}}^1 \frac{dz}{z^2} D_{c \rightarrow \pi}(z) \int_{x_{\min}}^1 \frac{dx}{x} \frac{1}{xS + U/z} \int \frac{dx'}{x'} \delta \left(x' - \frac{-xT/z}{xS + U/z} \right) \\ &\times q_a(x) \left[G(x') \hat{\sigma}_{ag \rightarrow c} + \sum_q q(x') \hat{\sigma}_{aq \rightarrow c} \right] , \end{aligned} \quad (33)$$

where \sum_a runs over up and down valence quarks, and \sum_q over quarks and antiquarks. In Eq. (33), the integration limits z_{\min} and x_{\min} , and variable x are given by

$$\begin{aligned} z_{\min} &= \frac{-(T + U)}{S} = \sqrt{x_F^2 + x_T^2} , \\ x_{\min} &= \frac{-U/z}{S + T/z} , \\ x' &= \frac{-x T/z}{x S + U/z} , \end{aligned} \quad (34)$$

where S, T, U are defined in Eq. (3), and x_F and x_T in Eq. (4). The short-distance partonic parts, $\hat{\sigma}_{ag \rightarrow c}$ and $\hat{\sigma}_{aq \rightarrow c}$, in Eq. (33), are given by [5]

$$\hat{\sigma}_{ag \rightarrow c} = \delta_{ac} \left[2 \left(1 - \frac{\hat{s}\hat{u}}{\hat{t}^2} \right) + \frac{4}{9} \left(\frac{-\hat{u}}{\hat{s}} + \frac{\hat{s}}{-\hat{u}} \right) + \left(\frac{\hat{s}}{\hat{t}} + \frac{\hat{u}}{\hat{t}} \right) \right] ; \quad (35a)$$

$$\begin{aligned} \hat{\sigma}_{aq \rightarrow c} &= \delta_{ac} \frac{4}{9} \left(\frac{\hat{s}^2 + \hat{u}^2}{\hat{t}^2} \right) + \delta_{qc} \frac{4}{9} \left(\frac{\hat{s}^2 + \hat{t}^2}{\hat{u}^2} \right) \\ &+ \delta_{aq} \delta_{qc} \frac{-8}{27} \left(\frac{\hat{s}^2}{\hat{u}\hat{t}} \right) + \delta_{a\bar{q}} \frac{4}{9} \left(\frac{\hat{t}^2 + \hat{u}^2}{\hat{s}^2} \right) , \end{aligned} \quad (35b)$$

where $\hat{s}, \hat{t}, \hat{u}$ are defined in Eq. (32).

Since we are interested in the large x_F region, we have $\ell^+ \gg \ell^-$ and $T \ll U \leq S$. Therefore, leading contributions to the cross section given in Eq. (33) come from the t -channel diagrams (the first diagrams in Fig. 9a and Fig. 9b), or equivalently, the $1/\hat{t}^2$ term (i.e., first term) in Eq. (35a) and Eq. (35b). Consequently, for leading contributions in the forward region, incoming parton a has the same flavor as fragmenting parton c . Therefore, in the valence quark approximation, we keep only $D_{u \rightarrow \pi^+}$ for π^+ production; $D_{d \rightarrow \pi^-}$ for π^- production, although we keep both $D_{u \rightarrow \pi^0}$ and $D_{d \rightarrow \pi^0}$ for π^0 production.

III. CALCULATION OF THE ASYMMETRY

In this section, we present our calculation of the single transverse-spin asymmetries in pion production in the valence quark-soft gluon approximation described in the previous section. We derive analytic expressions for the spin-dependent cross section, $\Delta\sigma(\ell, s_T)$, which is needed to evaluate the asymmetries.

A. Quark-Gluon Subprocesses with Initial-State Interactions

Consider the two diagrams with poles from initial-state interactions, as shown in Fig. 6a. We parameterize the parton momenta k_i as

$$k_1 = x_1 P + k_{1T}, \quad \text{and} \quad k_2 = x_2 P + k_{2T}, \quad (36)$$

with the k_{iT} two-dimensional transverse momenta. The remaining momentum components do not enter at twist three. The pole in the diagram at the left of Fig. 6a is given in these terms by

$$\frac{1}{(x'P' + k_2 - k_1)^2 + i\epsilon} \approx \frac{1}{(x_2 - x_1)x'S + (k_{2T} - k_{1T})^2 + i\epsilon}. \quad (37)$$

The derivative of this pole with respect to k_{2T} (or k_{1T}) vanishes as $k_{iT} \rightarrow 0$. The diagram on the right has the same feature. Therefore, following the arguments of Sec. II D above, the leading contribution to $\Delta\sigma(\vec{s}_T)$ in the diagrams in Fig. 6a is from the derivative of the phase space δ -function only.

Let L_1 and L_2 be the momenta of the unobserved partons in the diagrams to the left and right, respectively in Fig. 6a. We have

$$L_1 \equiv x'P' + x_1 P + k_{1T} - p_c, \quad L_2 \equiv x'P' + x_2 P + k_{2T} - p_c. \quad (38)$$

Taking the derivative with respect to k_1^ρ and k_2^ρ , we obtain

$$\frac{\partial}{\partial k_1^\rho} \delta(L_1^2) = (-2p_{c\rho})\delta'(L_1^2), \quad (39a)$$

$$\frac{\partial}{\partial k_2^\rho} \delta(L_1^2) = 0, \quad (39b)$$

$$\frac{\partial}{\partial k_1^\rho} \delta(L_2^2) = 0 , \quad (39c)$$

$$\frac{\partial}{\partial k_2^\rho} \delta(L_2^2) = (-2p_{c_\rho}) \delta'(L_2^2) . \quad (39d)$$

In deriving these relations, we have used that ρ is a transverse index. After taking the derivative with respect to the k_i on the δ -functions, we can set k_{i_T} to zero in the remainder of each diagram. For the diagrams in Fig. 6a, the poles giving the leading contributions are from

$$L(x_1, x_2) \equiv g_s [(2x' P' \cdot P) g_{\rho\beta} - (x' P')_\rho P_\beta - (x' P')_\beta P_\rho] \frac{-i}{[x' P' + (x_2 - x_1) P]^2 + i\epsilon} = g_s (-i) g_{\rho\beta} \left(\frac{-1}{x_1 - x_2 - i\epsilon} \right) , \quad (40a)$$

$$R(x_1, x_2) = g_s (-i) g_{\rho\beta} \left(\frac{-1}{x_2 - x_1 + i\epsilon} \right) , \quad (40b)$$

where L and R represent the diagrams at left and at right, respectively. In Eq. (40), $g_s = \sqrt{4\pi\alpha_s}$ is the strong coupling. In the following discussion, we absorb the overall $(-i)$ in Eq. (40) into the color factor for the subprocess. Using the distribution identity

$$\frac{1}{x_2 - x_1 \pm i\epsilon} = P \left[\frac{1}{x_2 - x_1} \right] \mp i\pi\delta(x_2 - x_1) , \quad (41)$$

for the poles in Eq. (40) and keeping the imaginary contribution of the pole, we can express the contributions of the diagrams in Fig. 6a as

$$\begin{aligned} & \frac{\partial}{\partial k_2^\rho} (H_{a_L}(x_1, x_2, x', p_c) + H_{a_R}(x_1, x_2, x', p_c)) \\ &= \frac{g_s}{2\pi x_2} H_{2 \rightarrow 2}(x_2, x', p_c) [i\pi\delta(x_1 - x_2)(2p_{c_\rho})] \delta'(L_2^2) , \end{aligned} \quad (42a)$$

$$\begin{aligned} & -\frac{\partial}{\partial k_1^\rho} (H_{a_L}(x_1, x_2, x', p_c) + H_{a_R}(x_1, x_2, x', p_c)) \\ &= \frac{g_s}{2\pi x_1} H_{2 \rightarrow 2}(x_1, x', p_c) [i\pi\delta(x_2 - x_1)(2p_{c_\rho})] \delta'(L_1^2) , \end{aligned} \quad (42b)$$

where subscripts a_L and a_R represent the left and right diagrams of Fig. 6a. In Eq. (42), $H_{2 \rightarrow 2}(x_i, x', p_c)$ with $i = 1, 2$ is proportional to the imaginary part of the $2 \rightarrow 2$ partonic forward scattering amplitude shown in Fig. 10,

$$H_{2 \rightarrow 2}(x_i, x', p_c) = \frac{1}{16\pi^2} \left| \overline{M}_{a+g \rightarrow c}^I \right|^2 C_g^I , \quad (43)$$

where the matrix element squared, $\left| \overline{M}_{a+g \rightarrow c}^I \right|^2$, is the same as that in Eq. (31), except for the color factor, C_g^I , due to the extra initial-state interaction. Combining Eqs. (19) and (40), the factor C_g^I is given by the color structure of the partonic diagrams shown in Fig. 6a, contracted with a common factor $[(-i)2/(N^2-1)](t^B)_{ij}$, where B and ij are color indices for the gluon and quarks from the polarized hadron. The factor $1/2\pi$ in Eq. (42) was explained

in the text following Eq. (18), and the factor $1/x_1$ is due to the definition of $H_{2 \rightarrow 2}(x_1, x', p_c)$, where incoming quark lines are contracted with $(1/2)\gamma \cdot (x_1 P)$. Eq. (42) shows that Eq. (30) is satisfied when $k_{i_T} = 0$.

Substituting Eq. (42a) into Eq. (29), we have a complete factorized form for the spin-dependent cross section from the diagrams shown in Fig. 6a,

$$E_\ell \frac{d\Delta\sigma_g^I(\vec{s}_T)}{d^3\ell} = \sum_{a,c} \int \frac{dz}{z^2} D_{c \rightarrow \pi}(z) \int dx' G(x') \int dx T_{F_a}^{(V)}(x, x) \left(E_c \frac{d\Delta\hat{\sigma}_{a+g \rightarrow c}^I(\vec{s}_T)}{d^3p_c} \right), \quad (44)$$

where the factor $1/z^2$ is due to the phase space difference between $d^3\ell/(2\pi)^3 2E_\ell$ and $d^3p_c/(2\pi)^3 2E_c$, and the partonic hard part, $E_c d\Delta\hat{\sigma}_{a+g \rightarrow c}^I/d^3p_c$, is given by

$$E_c \frac{d\Delta\hat{\sigma}_{a+g \rightarrow c}^I(\vec{s}_T)}{d^3p_c} = g_s \epsilon^{s_T p_c n \bar{n}} C_g^I \left[\frac{1}{16\pi^2 \hat{s}} \left| \bar{M}_{a+g \rightarrow c}^I \right|^2 \delta'(\hat{s} + \hat{t} + \hat{u}) \right]. \quad (45)$$

In Eqs. (44) and (45), superscript I indicates the contribution from a partonic subprocess with an initial-state pole, and subscript g represents the quark-gluon subprocess. In deriving Eq. (44), we renamed the integration variable x_1 in Eq. (42) as x . The factorized spin-dependent cross section given in Eq. (44) is very similar to the factorized form for the spin-averaged cross section in Eq. (16), with the unpolarized parton distribution $\phi_{a/A}(x)$ replaced by the twist-three correlation function $T_F^{(V)}(x, x)$. The partonic hard part in Eq. (45) is also very similar to that in Eq. (31). For the spin-dependent case, the derivative of the δ -function is just the derivative with respect to the parton momentum k_i in Eq. (20), which comes from the collinear expansion. The factor $\epsilon^{s_T p_c n \bar{n}}$ in Eq. (45) is necessary for a nonvanishing asymmetry.

After partial integration over x , we can reexpress the derivative of the δ -function as

$$\int dx \delta'(\hat{s} + \hat{t} + \hat{u}) F(x) = \int \frac{dx}{x'S + T/z} \delta(\hat{s} + \hat{t} + \hat{u}) \left[-\frac{\partial}{\partial x} F(x) \right] \quad (46)$$

for any smooth function $F(x)$. Using Eq. (45), we thus rewrite $E_\ell d\Delta\sigma_g^I(s_T)/d^3\ell$ as

$$E_\ell \frac{d\Delta\sigma_g^I(\vec{s}_T)}{d^3\ell} = \frac{\alpha_s^2}{S} \sum_{a,c} \int_{z_{\min}}^1 \frac{dz}{z^3} D_{c \rightarrow \pi}(z) \int_{x_{\min}}^1 \frac{dx}{x} \frac{1}{xS + U/z} \int \frac{dx'}{x'} \delta \left(x' - \frac{-xT/z}{xS + U/z} \right) \times g_s \epsilon^{s_T \ell n \bar{n}} \left(\frac{1}{x'S + T/z} \right) G(x') \left[-x \frac{\partial}{\partial x} \left(\frac{T_{F_a}^{(V)}(x, x)}{x} H_{a \rightarrow c}^I(\hat{s}, \hat{t}, \hat{u}) \right) \right], \quad (47)$$

where z_{\min} and x_{\min} are given in Eq. (34), and S, T and U are defined in Eq. (3). In Eq. (47), the spin-dependent cross section $E_\ell d\Delta\sigma_g^I(s_T)/d^3\ell$ has almost the same factorized form as the spin-averaged cross section shown in Eq. (33). The extra factor of $1/z$ is due to the replacement of p_c by ℓ in the ϵ -tensor of Eq. (45). The dimension of $1/(x'S + T/z)$ due to the derivative of the δ -function is balanced by the dimension of ℓ in the ϵ -tensor and the dimension of the twist-three correlation function $T_{F_a}^{(V)}(x, x)$. In our definition, the twist-three correlation function has the dimensions of energy. The partonic hard part, $H_{a \rightarrow c}^I(\hat{s}, \hat{t}, \hat{u})$, in Eq. (47) plays the role of $\hat{\sigma}_{a \rightarrow c}$ in Eq. (33). It is given by $C_g^I |\bar{M}_{a+g \rightarrow c}^I|^2$ in Eq. (45), which represents the $2 \rightarrow 2$ matrix element squared in Eq. (43), but with a different color factor due to the extra initial-state interaction.

B. Quark-Gluon Subprocesses with Final-State Interactions

The diagrams shown in Fig. 6b represent final-state interactions of the fragmenting parton. As with the contributions from initial-state interactions, these diagrams also have a derivative with respect to k_1^ρ and k_2^ρ of the phase space δ -function associated with the unobserved final-state parton, of momentum L_1 or L_2 . Similarly to Eq. (40), the final-state poles giving leading contributions are given by, as sketched in Fig. 11,

$$L(x_1, x_2) \equiv g_s (\gamma \cdot p_c) \frac{\gamma \cdot P \gamma \cdot (p_c + (x_1 - x_2)P)}{(p_c + (x_1 - x_2)P)^2 + i\epsilon} \approx g_s (\gamma \cdot p_c) \left(\frac{1}{x_1 - x_2 + i\epsilon} \right), \quad (48a)$$

$$R(x_1, x_2) \approx g_s (\gamma \cdot p_c) \left(\frac{1}{x_2 - x_1 - i\epsilon} \right), \quad (48b)$$

where the factor $(\gamma \cdot p_c)$ will be absorbed into the $2 \rightarrow 2$ hard-scattering function. Similarly to Eq. (47), we obtain the contribution from the derivative of the δ -function for a final-state interaction,

$$E_\ell \frac{d\Delta\sigma_g^F(\vec{s}_T)}{d^3\ell} = \frac{\alpha_s^2}{S} \sum_{a,c} \int_{z_{\min}}^1 \frac{dz}{z^3} D_{c \rightarrow \pi}(z) \int_{x_{\min}}^1 \frac{dx}{x} \frac{1}{xS + U/z} \int \frac{dx'}{x'} \delta \left(x' - \frac{-xT/z}{xS + U/z} \right) \times g_s \epsilon^{s_T \ell n \bar{n}} \left(\frac{1}{x'S + T/z} \right) G(x') \left[-x \frac{\partial}{\partial x} \left(\frac{T_{F_a}^{(V)}(x, x)}{x} H_{ag \rightarrow c}^F(\hat{s}, \hat{t}, \hat{u}) \right) \right], \quad (49)$$

where superscript F denotes the final-state interaction. The only difference between $E_\ell d\Delta\sigma_g^F(s_T)/d^3\ell$ in Eq. (49) and $E_\ell d\Delta\sigma_g^I(s_T)/d^3\ell$ in Eq. (47) is the color factors in the partonic hard parts. The hard part $H_{ag \rightarrow c}^F(\hat{s}, \hat{t}, \hat{u})$ in Eq. (49) is given by $C_g^F |\overline{M}_{a+g \rightarrow c}^I|^2$, which has the same kinematic dependence as $H_{ag \rightarrow c}^I(\hat{s}, \hat{t}, \hat{u})$ in Eq. (47), but a different color factor, C_g^F , due to different color structures in final-state compared to initial-state interactions. Similarly to C_g^I , C_g^F is computed by contracting the matrix $[2/(N^2 - 1)](t^B)_{ij}$, Eq. (19), into the diagrams.

In addition to the contribution from the derivative of the δ -function, the diagrams shown in Fig. 6b also give leading contributions, proportional to $(\partial/\partial x)T_F^{(V)}(x, x)$, from the double pole which results when the derivative $(\partial/\partial k_i)$ acts on a propagator that goes on-shell at $x_1 = x_2$. Consider the final-state interaction in the diagram at the left in Fig. 11a. The pole giving the leading contribution is from the factor

$$L(k_{1_T}, k_{2_T}) \equiv g_s \gamma \cdot p_c \left[\frac{\gamma \cdot P \gamma \cdot (p_c + k_1 - k_2)}{(p_c + k_1 - k_2)^2 + i\epsilon} \right] = g_s \gamma \cdot p_c \left[\frac{1}{x_1 - x_2 + x_0(k_{1_T}, k_{2_T}) + i\epsilon} - \frac{\gamma \cdot (k_{1_T} - k_{2_T}) \gamma \cdot P}{2P \cdot p_c [x_1 - x_2 + x_0(k_{1_T}, k_{2_T}) + i\epsilon]} \right], \quad (50)$$

where x_0 is defined as

$$x_0(k_{1T}, k_{2T}) \equiv \frac{2(k_{1T} - k_{2T}) \cdot p_c + (k_{1T} - k_{2T})^2}{2P \cdot p_c} \rightarrow 0 \quad \text{as } k_{1T} \text{ and } k_{2T} \rightarrow 0. \quad (51)$$

In deriving Eq. (50), we used the parameterization of Eq. (36), and the relations $p_c^2 = 0$, $P^2 \approx 0$, and $2P \cdot p_c > 0$. Applying $(\partial/\partial k_i^\rho)$ to $L(k_{1T}, k_{2T})$, and letting k_{iT} ($i = 1, 2$) go to zero, the first term in Eq. (50) develops a double pole, while the second term remains a single pole,

$$\begin{aligned} \frac{\partial}{\partial k_1^\rho} L(k_{1T} = 0, k_{2T} = 0) &= \gamma \cdot p_c \left(\frac{g_s}{2P \cdot p_c} \right) \left[(-2p_{c_\rho}) \frac{1}{(x_1 - x_2 + i\epsilon)^2} \right. \\ &\quad \left. - (\gamma_\rho \gamma \cdot P) \frac{1}{(x_1 - x_2 + i\epsilon)} \right] \\ &= -\frac{\partial}{\partial k_2^\rho} L(k_{1T} = 0, k_{2T} = 0). \end{aligned} \quad (52)$$

Since we keep only contributions proportional to $(\partial/\partial x)T_F^{(V)}(x, x)$, we neglect the single-pole term in Eq. (52) in the following discussion, and use

$$\begin{aligned} \frac{\partial}{\partial k_2^\rho} L(k_{1T} = 0, k_{2T} = 0) &= -\frac{\partial}{\partial k_1^\rho} L(k_{1T} = 0, k_{2T} = 0) \\ &\approx \gamma \cdot p_c \left(\frac{g_s}{2P \cdot p_c} \right) \left[(2p_{c_\rho}) \frac{1}{(x_1 - x_2 + i\epsilon)^2} \right]. \end{aligned} \quad (53)$$

Similarly, for the diagram at the right in Fig. 11b, we have

$$\begin{aligned} R(k_{1T}, k_{2T}) &\equiv g_s \left[\frac{\gamma \cdot (p_c + k_2 - k_1) \gamma \cdot P}{(p_c + k_2 - k_1)^2 - i\epsilon} \right] \gamma \cdot p_c \\ &= g_s \left[\frac{1}{x_2 - x_1 + x_0(k_{2T}, k_{1T}) - i\epsilon} \right. \\ &\quad \left. - \frac{\gamma \cdot P \gamma \cdot (k_{2T} - k_{1T})}{2P \cdot p_c [x_2 - x_1 + x_0(k_{2T}, k_{1T}) - i\epsilon]} \right] \gamma \cdot p_c, \end{aligned} \quad (54)$$

where x_0 is defined in Eq. (51). Taking the derivative with respect to k_i^ρ , we have

$$\begin{aligned} \frac{\partial}{\partial k_2^\rho} R(k_{1T} = 0, k_{2T} = 0) &= -\frac{\partial}{\partial k_1^\rho} R(k_{1T} = 0, k_{2T} = 0) \\ &\approx \gamma \cdot p_c \left(\frac{g_s}{2P \cdot p_c} \right) \left[(-2p_{c_\rho}) \frac{1}{(x_2 - x_1 - i\epsilon)^2} \right]. \end{aligned} \quad (55)$$

Eqs. (53) and (55) show that the double-pole contributions from diagrams in Fig. 6b satisfy Eq. (30). Keeping only these double-pole terms, as in Eq. (42a), we now have

$$\frac{\partial H_{D_L}}{\partial k_2^\rho}(x_1, x_2, x', p_c) \approx \frac{g_s}{2\pi} H_{2 \rightarrow 2}^L(x_1, x_2, x', p_c) \left[(2p_{c_\rho}) \frac{1}{(x_1 - x_2 + i\epsilon)^2} \right] \left(\frac{1}{2P \cdot p_c} \right), \quad (56a)$$

$$\frac{\partial H_{D_R}}{\partial k_2^\rho}(x_1, x_2, x', p_c) \approx \frac{g_s}{2\pi} H_{2 \rightarrow 2}^R(x_1, x_2, x', p_c) \left[(-2p_{c_\rho}) \frac{1}{(x_2 - x_1 - i\epsilon)^2} \right] \left(\frac{1}{2P \cdot p_c} \right), \quad (56b)$$

where D_L and D_R denote the double-pole contributions from the left and right diagram in Fig. 6b, respectively. In Eq. (56), $H_{2 \rightarrow 2}^L(x_1, x_2, x', p_c)$ and $H_{2 \rightarrow 2}^R(x_1, x_2, x', p_c)$ are $2 \rightarrow 2$ partonic parts corresponding to the left and right diagrams shown in Fig. 12. They have the limits

$$H_{2 \rightarrow 2}^L(x_1, x_2, x', p_c)_{x_1 \rightarrow x_2} = \frac{1}{x_2} H_{2 \rightarrow 2}(x_2, x', p_c) , \quad (57a)$$

$$H_{2 \rightarrow 2}^R(x_1, x_2, x', p_c)_{x_2 \rightarrow x_1} = \frac{1}{x_1} H_{2 \rightarrow 2}(x_1, x', p_c) , \quad (57b)$$

where $H_{2 \rightarrow 2}(x_i, x', p_c)$ with $i = 1, 2$ are the same as in Eq. (42).

Recalling that T_F is real, it is evident from Eq. (29) that we need the imaginary part of $(\partial/\partial k_2^\rho)H_{D_L}$ and $(\partial/\partial k_2^\rho)H_{D_R}$ in order to get a real contribution to the spin-dependent cross section. For double pole terms like those in Eq. (56a) and (56b), the imaginary part is given by

$$\int dx_1 \frac{1}{(x_1 - x_2 + i\epsilon)^2} F(x_1, x_2) = \int dx_1 [-i\pi \delta(x_1 - x_2)] \left[\frac{\partial}{\partial x_1} F(x_1, x_2) \right] \quad (58)$$

for any smooth function $F(x_1, x_2)$. Using Eq. (57), we have following relation,

$$\begin{aligned} & \int dx_1 dx_2 T_{F_a}^{(V)}(x_1, x_2) \left[i\epsilon^{\rho s_T n \bar{n}} \frac{\partial}{\partial k_2^\rho} (H_{D_L}(x_1, x_2, x', p_c) + H_{D_R}(x_1, x_2, x', p_c)) \right] \\ &= g_s \frac{\epsilon^{s_T p_c n \bar{n}}}{2P \cdot p_c} \left\{ \int dx_2 \left[-\frac{\partial}{\partial x_1} (H_{2 \rightarrow 2}^L(x_1, x_2, x', p_c) T_{F_a}^{(V)}(x_1, x_2)) \right]_{x_1=x_2} \right. \\ & \quad \left. + \int dx_1 \left[-\frac{\partial}{\partial x_2} (H_{2 \rightarrow 2}^R(x_1, x_2, x', p_c) T_{F_a}^{(V)}(x_1, x_2)) \right]_{x_2=x_1} \right\} \\ & \approx g_s \frac{\epsilon^{s_T \ell n \bar{n}}}{2P \cdot \ell} \int \frac{dx}{x} H_{2 \rightarrow 2}(x, x', p_c) \left[-\frac{\partial}{\partial x} (T_{F_a}^{(V)}(x, x)) \right] . \end{aligned} \quad (59)$$

In deriving Eq. (59), we have used the symmetry property $T_F^{(V)}(x_1, x_2) = T_F^{(V)}(x_2, x_1)$, Eq. (26), [10]

$$\frac{\partial}{\partial x} (T_{F_a}^{(V)}(x, x)) = 2 \left[\frac{\partial}{\partial x_1} (T_{F_a}^{(V)}(x_1, x)) \right]_{x_1=x} = 2 \left[\frac{\partial}{\partial x_2} (T_{F_a}^{(V)}(x, x_2)) \right]_{x_2=x} , \quad (60a)$$

and Eq. (57). In addition, we have used the approximation

$$\begin{aligned} & \left[-\frac{\partial}{\partial x_1} (H_{2 \rightarrow 2}^L(x_1, x_2, x', p_c) T_{F_a}^{(V)}(x_1, x_2)) \right]_{x_1=x_2} \\ & \approx \frac{1}{x_2} H_{2 \rightarrow 2}(x_2, x', p_c) \left[-\frac{\partial}{\partial x_1} (T_{F_a}^{(V)}(x_1, x_2)) \right]_{x_1=x_2} , \end{aligned} \quad (61)$$

demanding as usual a derivative of $T_F^{(V)}$.

Substituting Eq. (59) into the cross section Eq. (29), we obtain the leading double-pole contributions from the diagrams shown in Fig. 6b

$$E_\ell \frac{d\Delta\sigma_g^D(\vec{s}_T)}{d^3\ell} = \frac{\alpha_s^2}{S} \sum_{a,c} \int_{z_{\min}}^1 \frac{dz}{z^2} D_{c \rightarrow \pi}(z) \int_{x_{\min}}^1 \frac{dx}{x} \frac{1}{xS+U/z} \int \frac{dx'}{x'} \delta\left(x' - \frac{-xT/z}{xS+U/z}\right) \times g_s \epsilon^{s_T \ell n \bar{n}} \left(\frac{1}{-T} \right) G(x') \left[-\frac{\partial}{\partial x} \left(T_{F_a}^{(V)}(x, x') \right) \right] H_{ag \rightarrow c}^D(\hat{s}, \hat{t}, \hat{u}), \quad (62)$$

where $T = -2P \cdot \ell$ is defined in Eq. (3), and the partonic hard part $H_{ag \rightarrow c}^D(\hat{s}, \hat{t}, \hat{u})$ is normalized to have

$$H_{ag \rightarrow c}^D(\hat{s}, \hat{t}, \hat{u}) = H_{ag \rightarrow c}^F(\hat{s}, \hat{t}, \hat{u}), \quad (63)$$

with $H_{ag \rightarrow c}^F(\hat{s}, \hat{t}, \hat{u})$ the same partonic hard part derived from the contribution of the derivative of the δ -function, and given in Eq. (49).

In addition to the diagrams in Fig. 6b, there is another type of diagram with final-state interactions, as shown in Fig. 6c. In this case the final-state interactions taken place on an unobserved final-state parton. The diagrams on the left and right are the same, except for the final-state propagator and the argument of the phase space δ -function. The total partonic contribution from these two diagrams can be expressed as

$$H_{cL}(k_1, k_2, x', p_c) + H_{cR}(k_1, k_2, x', p_c) = \left[\frac{1}{L_1^2 + i\epsilon} \delta(L_2^2) + \frac{1}{L_2^2 - i\epsilon} \delta(L_1^2) \right] F(k_1, k_2, x', p_c), \quad (64)$$

where the momenta L_1 and L_2 are defined in Eq. (38). The function $F(k_1, k_2, x', p_c)$ represents the common factor of two diagrams in Fig. 6c; it has the symmetry property

$$F(k_1, k_2, x', p_c) = F(k_2, k_1, x', p_c). \quad (65)$$

From Eq. (64), combining the symmetry properties of Eqs. (26) and (65), we readily show that the leading contribution of the diagrams in Fig. 6c to the spin-dependent cross section (or Eq. (29)) vanishes.

C. Quark-Quark and Quark-Antiquark Subprocesses

In this subsection, we present the leading contributions to the spin-dependent cross section from quark-quark and quark-antiquark subprocesses.

Based on the same arguments following Eq. (37), the leading contributions from diagrams with initial-state interactions, shown in Fig. 13a, come only from the derivative of the phase space δ -function. By analogy to Eq. (47), we obtain

$$E_\ell \frac{d\Delta\sigma_q^I(\vec{s}_T)}{d^3\ell} = \frac{\alpha_s^2}{S} \sum_{a,c} \int_{z_{\min}}^1 \frac{dz}{z^3} D_{c \rightarrow \pi}(z) \int_{x_{\min}}^1 \frac{dx}{x} \frac{1}{xS+U/z} \int \frac{dx'}{x'} \delta\left(x' - \frac{-xT/z}{xS+U/z}\right) \times g_s \epsilon^{s_T \ell n \bar{n}} \left(\frac{1}{x'S+T/z} \right) \sum_q q(x') \left[-x \frac{\partial}{\partial x} \left(\frac{T_{F_a}^{(V)}(x, x')}{x} H_{aq \rightarrow c}^I(\hat{s}, \hat{t}, \hat{u}) \right) \right], \quad (66)$$

where the partonic hard part, $H_{aq \rightarrow c}^I(\hat{s}, \hat{t}, \hat{u})$ is given by the $2 \rightarrow 2$ quark-quark (quark-antiquark) diagrams shown in Fig. 14. Compared to the spin-averaged case, $H_{aq \rightarrow c}^I(\hat{s}, \hat{t}, \hat{u})$

plays the same role as $\hat{\sigma}_{aq \rightarrow c}$ in Eq. (33). In fact, $H_{aq \rightarrow c}^I(\hat{s}, \hat{t}, \hat{u})$ is given by the same Feynman diagrams needed to calculate $\hat{\sigma}_{aq \rightarrow c}$, but, with different color factors, C_q^I , due to the extra initial-state interactions. Similarly to C_g^I , C_q^I is given by the color structures of the diagrams shown in Fig. 13a, contracted with $[2/(N^2 - 1)](t^B)_{ij}$, where B and ij are color indices for the gluon and quarks from the polarized hadron, respectively.

Contributions from the derivatives of the phase space δ -functions of the diagrams with final-state interactions shown in Fig. 13b are given by

$$E_\ell \frac{d\Delta\sigma_q^F(\vec{s}_T)}{d^3\ell} = \frac{\alpha_s^2}{S} \sum_{a,c} \int_{z_{\min}}^1 \frac{dz}{z^3} D_{c \rightarrow \pi}(z) \int_{x_{\min}}^1 \frac{dx}{x} \frac{1}{xS + U/z} \int \frac{dx'}{x'} \delta\left(x' - \frac{-xT/z}{xS + U/z}\right) \times g_s \epsilon^{s_T \ell n \bar{n}} \left(\frac{1}{x'S + T/z}\right) \sum_q q(x') \left[-x \frac{\partial}{\partial x} \left(\frac{T_{F_a}^{(V)}(x, x)}{x} H_{aq \rightarrow c}^F(\hat{s}, \hat{t}, \hat{u}) \right) \right], \quad (67)$$

where superscript F represents the final-state interactions. The partonic hard-scattering function, $H_{aq \rightarrow c}^F(\hat{s}, \hat{t}, \hat{u})$, has the same functional form as $H_{aq \rightarrow c}^I(\hat{s}, \hat{t}, \hat{u})$ in Eq. (66), with a different color factor C_q^F , because of the final-state interactions. As with C_g^F , C_q^F is given by the color structure of the diagrams shown in Fig. 13b, contracted with $[2/(N^2 - 1)](t^B)_{ij}$.

In addition to the contributions given in Eq. (67) from the derivative of the δ -function, the diagrams in Fig. 13b also have leading contributions from double-pole terms. Just as for the contributions from the quark-gluon subprocesses, given in Eq. (62), the quark-quark and quark-antiquark double-pole contributions take the form

$$E_\ell \frac{d\Delta\sigma_q^D(\vec{s}_T)}{d^3\ell} = \frac{\alpha_s^2}{S} \sum_{a,c} \int_{z_{\min}}^1 \frac{dz}{z^2} D_{c \rightarrow \pi}(z) \int_{x_{\min}}^1 \frac{dx}{x} \frac{1}{xS + U/z} \int \frac{dx'}{x'} \delta\left(x' - \frac{-xT/z}{xS + U/z}\right) \times g_s \epsilon^{s_T \ell n \bar{n}} \left(\frac{1}{-T}\right) \sum_q q(x') \left[-\frac{\partial}{\partial x} (T_{F_a}^{(V)}(x, x)) \right] H_{aq \rightarrow c}^D(\hat{s}, \hat{t}, \hat{u}), \quad (68)$$

where the hard-scattering function found from the double pole, $H_{aq \rightarrow c}^D(\hat{s}, \hat{t}, \hat{u})$ is equal to $H_{aq \rightarrow c}^F(\hat{s}, \hat{t}, \hat{u})$ in Eq. (67).

D. Calculation of the Partonic Hard Scattering Functions

In Eqs. (47), (49), (62), (66), (67) and (68), we have presented factorized expressions for leading contributions to the spin-dependent cross section, $E_\ell d\Delta\sigma(\vec{s}_T)/d^3\ell$, for quark-gluon, quark-quark and quark-antiquark subprocesses. To complete our derivation of the spin-dependent cross section, in this subsection we outline the calculation of the partonic hard scattering functions $H_{ag \rightarrow c}^I$, $H_{ag \rightarrow c}^F$, $H_{aq \rightarrow c}^I$ and $H_{aq \rightarrow c}^F$. We recall that the subscripts I and F refer to initial- and final-state interactions, respectively. The other two hard scattering functions, associated with derivatives on final-state propagators only, $H_{ag \rightarrow c}^D$ and $H_{aq \rightarrow c}^D$, are equal to $H_{ag \rightarrow c}^F$ and $H_{aq \rightarrow c}^F$, respectively.

For the quark-gluon subprocesses, the partonic hard scattering functions $H_{ag \rightarrow c}^I$ and $H_{ag \rightarrow c}^F$ are given by the same quark-gluon $2 \rightarrow 2$ Feynman diagrams as shown in Fig. 15, which are actually the same diagrams contributing to the spin-averaged partonic part, $\hat{\sigma}_{ag \rightarrow c}$, in Eq. (35a). Incoming quark lines are contracted by $(1/2)\gamma \cdot (xP)$, and incoming gluon lines are contracted by $(1/2)(-g_{\alpha\beta})$.

Let C_g , C_g^I , and C_g^F be the color factors for processes that are spin-averaged, spin-dependent with an initial-state interaction, and spin-dependent with a final-state interaction, respectively. The factor C_g for each diagram shown in Fig. 15 is simply the standard color factor for that diagram, with an average over initial-state quark and gluon color.

Each C_g^I is given by the color factor of the diagram with one extra initial-state three-gluon vertex. An example is shown in Fig. 16a. The color of the incoming gluon from the unpolarized hadron is averaged, and the colors of the incoming quarks and the extra gluon from the polarized hadron are contracted with $[-2i/(N^2 - 1)](t^B)_{ij}$, as explained in the text following Eq. (43).

Finally, the C_g^F are the color factors of the same $2 \rightarrow 2$ diagrams with an extra final-state quark-gluon interaction, illustrated by the diagram shown in Fig. 16b. Similarly to C_g^I , the color of the incoming gluon from the unpolarized hadron is averaged, and the colors of the incoming quarks and the extra gluon from the polarized hadron are contracted with $[2/(N^2 - 1)](t^B)_{ij}$, as mentioned in the text after Eq. (49). Our results for all these color factors are collected in Table I.

For quark-quark (or quark-antiquark) subprocesses, the partonic hard scattering functions, $H_{aq \rightarrow c}^I$ and $H_{aq \rightarrow c}^F$ are given by the same quark-quark (or quark-antiquark) $2 \rightarrow 2$ Feynman diagrams as shown in Fig. 17, which are the same diagrams contributing to the spin-averaged partonic cross section, $\hat{\sigma}_{aq \rightarrow c}$ in Eq. (35b). Incoming quark lines from the polarized hadron are contracted by $(1/2)\gamma \cdot (xP)$, and incoming quark (or antiquark) lines from the unpolarized hadron are contracted by $(1/2)\gamma \cdot (x'P')$.

As with the quark-gluon subprocesses, C_q , C_q^I , and C_q^F are respectively the color factors for subprocesses that are spin-averaged, spin-dependent with an initial-state interaction, and spin-dependent with a final-state interaction. The C_q for the individual diagrams shown in Fig. 17 are the color factors for each diagram, with a standard average over initial-state quark (or antiquark) color. The C_q^I 's are found by including an extra initial-state three-gluon interaction in the $2 \rightarrow 2$ process, (for example, Fig. 18a) averaging the color of the quark (or antiquark) from the unpolarized hadron, and contracting the colors of the incoming quarks and the extra gluon from the polarized hadron with $[2/(N^2 - 1)](t^B)_{ij}$, as mentioned following Eq. (66). The C_q^F are found from the same $2 \rightarrow 2$ diagrams, now with one extra final-state quark-gluon interaction (illustrated by the diagram shown in Fig. 18b). In exactly the same fashion as for C_q^I , the colors from the unpolarized hadron are averaged, and the colors from the polarized hadron are contracted with $[2/(N^2 - 1)](t^B)_{ij}$ (as mentioned in connection with Eq. (67)).

Our results for the quark-quark and quark-antiquark color factors are summarized in Table II. Notice the sign difference for the coefficient of $4N$ in the color factor $(N^2 \pm 4N - 4)/(32N)$, between graphs related by reversing the arrow of a quark or antiquark line. These will give slight differences to the asymmetries in proton(\uparrow)-proton compared with antiproton(\uparrow)-proton collisions.

From Table I and Table II, we can construct all the necessary partonic hard scattering functions. For the spin-averaged cross section, the hard-scattering function for the quark-gluon subprocess, $\hat{\sigma}_{aq \rightarrow c}$ in Eq. (35a), is found by combining the entries in the columns of *Partonic Parts* and C_g in Table I. For the quark-quark (or antiquark) subprocesses, $\hat{\sigma}_{aq \rightarrow c}$ in Eq. (35b) is found by combining entries from the columns of *Partonic Parts* with C_q in Table II. For the spin-dependent cross section, the twist-three partonic hard scattering

function $H_{ag \rightarrow c}^I$ is found by combining entries in the columns of *Partonic Parts* and C_g^I in Table I. In the same way, one can read off other partonic hard scattering functions, $H_{ag \rightarrow c}^F$, $H_{aq \rightarrow c}^I$ and $H_{aq \rightarrow c}^F$ from Table I and Table II.

IV. NUMERICAL RESULTS FOR SINGLE TRANSVERSE-SPIN ASYMMETRIES

Having derived expressions for the single transverse-spin asymmetries in previous section, we are now ready to develop numerical estimates of A_N for inclusive single pion production.

A. Model for the Twist-3 Distribution: $T_F^{(V)}(x, x)$

The application of perturbative QCD to observables involving hadrons in the initial state relies on factorization theorems [31] and on the universality of the nonperturbative, long-distance distributions. For the single transverse-spin asymmetries discussed in this paper, a test of the perturbative formalism requires in principle an independent extraction of the spin-dependent twist-three distributions, $\phi_{a/A}^{(3)}(x_1, x_2)$ introduced in Eq. (17). As we have observed, there are a variety of twist-three distributions, dependent in general on a pair of momentum fractions. It would require extensive measurements to pin down all of these functions. However, for single-spin asymmetries in the forward region, we have argued above, and in Ref. [10], that the dominant contribution may depend primarily on only a single twist-three distribution, $T_{F_a}^{(V)}(x, x)$, at equal values of its two arguments. Assuming this to be the case, it could be possible to infer the form of $T_{F_a}^{(V)}(x, x)$ from single transverse-spin asymmetries in π^+ and/or π^- production, and then use it to predict asymmetries in the production of π^0 , direct photon or other particles, at least approximately.

In order to compare our calculated asymmetries to the existing data, we need to assume an initial functional form for the twist-3 distribution, $T_{F_a}^{(V)}(x, x)$. To help motivate our model, we compare the operator definition of $T_{F_a}^{(V)}(x, x)$ with that of a twist-2 quark distribution $q_a(x)$ of flavor a . From Eq. (25), we have

$$T_{F_a}^{(V)}(x, x) = \int \frac{dy^-}{4\pi} e^{ixP^+y^-} \langle P, \vec{s}_T | \bar{\psi}_a(0) \gamma^+ \times \left[\int dy_2^- \epsilon^{s_T \sigma n \bar{n}} F_{\sigma+}(y_2^-) \right] \psi_a(y^-) | P, \vec{s}_T \rangle , \quad (69)$$

where subscript a is quark flavor. Correspondingly, from Ref. [39] we have for the quark distribution

$$q_a(x) = \int \frac{dy^-}{4\pi} e^{ixP^+y^-} \langle P | \bar{\psi}_a(0) \gamma_+ \psi_a(y^-) | P \rangle . \quad (70)$$

As above, we suppress ordered exponentials of the gauge field. Comparing Eqs. (69) with (70), the operator defining $T_{F_a}^{(V)}(x, x)$ is the same as for the spin-averaged quark distribution, except for the term in the square brackets. This factor, however, does not introduce explicit x -dependence (or y -dependence in coordinate space). Based on this similarity of the

operators, we model the twist-3 distribution with the following functional form, inspired by the quark distributions themselves,

$$T_{F_a}^{(V)}(x, x) \equiv \kappa_a \lambda q_a(x) , \quad (71)$$

where λ (with dimensions of energy) is a normalization constant, which will be fixed by the data; and where $\kappa_a = \pm 1, 0$, depending on flavor a . Note that we propose the relation Eq. (71) only for relatively large x , where the correlations of quarks with the gluon field may be simplified. This restriction limits somewhat the utility of low moments of T_F in estimates of its magnitude [13].

For the parameters κ_a in Eq. (71), we shall see that the data suggest the choices

$$\begin{aligned} \kappa_u &= +1 \quad \text{and} \quad \frac{\kappa_u}{\kappa_d} = -1 \quad (\text{proton}) , \\ \kappa_{\bar{u}} &= -1 \quad \text{and} \quad \frac{\kappa_{\bar{u}}}{\kappa_{\bar{d}}} = -1 \quad (\text{antiproton}) , \end{aligned} \quad (72)$$

where the second line follows from the first by using charge conjugation invariance in T_F . In the valence quark approximation, discussed in the previous sections, we further assume that $\kappa_s = 0$. Of course, Eq. (71) is simply a model, and the true functional form of the twist-three distribution $T_{F_a}^{(V)}(x, x)$ should be determined by detailed comparison with experiment. The purpose of our model is to have a functional form that we can use to begin such a comparison with the important, but still limited, data that are available.

B. Single Transverse-spin Asymmetries in Pion Production

Single transverse-spin asymmetries for pions were been measured at Fermilab by the E704 Collaboration with 200 GeV polarized proton and antiproton beams on an unpolarized proton target [4]. In this subsection, we use the Fermilab data to estimate the value of λ , in Eq. (71), and check the consistency of our model.

1. Absolute Sign of the Single Transverse-Spin Asymmetry

In order to compare the experimental data on the asymmetries, A_N , with our calculations in Sec. III, we need to fix the absolute sign of A_N .

According to Ref. [4], positive values of A_N correspond to larger cross sections for production of π^0 to the beam's *left* when the beam particle spin is vertically *upward*, as sketched in Fig. 19. We choose our coordinate system such that the beam direction is along the z -axis, and the direction of the beam spin is along the x -axis, as shown in Fig. 19. Consequently, the experimental beam's *left* corresponds to the $-y$ -direction in our coordinate system, and

$$(A_N)_{\text{exp}} > 0 \iff \epsilon^{\ell_T s_T n \bar{n}} > 0 . \quad (73)$$

Eq. (73) fixes the absolute sign of A_N presented in Sec. III, and dictates our choice $\kappa_u = +1$ in Eq. (72).

2. Leading Single Transverse-Spin Asymmetry $[(\partial/\partial x)T_{F_a}^{(V)}(x, x) \text{ only}]$

As explained in Sec. III, we are interested in A_N in the forward region, where it is largest experimentally. In deriving Eqs. (47), (49), (62), (66), (67) and (68), we kept only contributions from the terms discussed in items (1) and (2) of Sec. II D, because those discussed in items (3) and (4) lack a derivative on the twist-three distribution. To be consistent with our approximation, we rewrite the contributions in Eqs. (47), (49), (62), (66), (67) and (68) in terms of an explicit factor of $(\partial/\partial x)T_{F_a}^{(V)}(x, x)$, neglecting derivatives of other factors. Combining all leading contributions to the spin-dependent cross section, in a manner similar to the spin-averaged cross section in Eq. (33), we obtain

$$E_\ell \frac{d^3 \Delta\sigma(\vec{s}_T)}{d^3 \ell} = \frac{\alpha_s^2}{S} \sum_{a,c} \int_{z_{\min}}^1 \frac{dz}{z^2} D_{c \rightarrow \pi}(z) \int_{x_{\min}}^1 \frac{dx}{x} \frac{1}{xS + U/z} \int \frac{dx'}{x'} \delta\left(x' - \frac{-xT/z}{xS + U/z}\right) \quad (74)$$

$$\times \sqrt{4\pi\alpha_s} \left(\frac{\epsilon^{s_T \ell n \bar{n}}}{z(-\hat{u})} \right) \left[-x \frac{\partial}{\partial x} T_{F_a}^{(V)}(x, x) \right] \left[G(x') \Delta\hat{\sigma}_{ag \rightarrow c} + \sum_q q(x') \Delta\hat{\sigma}_{aq \rightarrow c} \right] ,$$

where \sum_a runs over up and down valence quarks. The integration limits in Eq. (74) are the same as those defined in Eq. (33). The spin-dependent partonic cross sections, $\Delta\hat{\sigma}_{ag \rightarrow c}$ and $\Delta\hat{\sigma}_{aq \rightarrow c}$ are given by

$$\Delta\hat{\sigma}_{ag \rightarrow c} = - \left[H_{ag \rightarrow c}^I(\hat{s}, \hat{t}, \hat{u}) + H_{ag \rightarrow c}^F(\hat{s}, \hat{t}, \hat{u}) + \left(\frac{\hat{u}}{\hat{t}} \right) H_{ag \rightarrow c}^D(\hat{s}, \hat{t}, \hat{u}) \right] , \quad (75a)$$

$$\Delta\hat{\sigma}_{aq \rightarrow c} = - \left[H_{aq \rightarrow c}^I(\hat{s}, \hat{t}, \hat{u}) + H_{aq \rightarrow c}^F(\hat{s}, \hat{t}, \hat{u}) + \left(\frac{\hat{u}}{\hat{t}} \right) H_{aq \rightarrow c}^D(\hat{s}, \hat{t}, \hat{u}) \right] , \quad (75b)$$

where the minus sign is from $\epsilon^{s_T \ell n \bar{n}} = -\epsilon^{s_T \ell n \bar{n}}$, and where all the partonic hard-scattering functions have been given in Sec. III. In deriving Eq. (75), $(x'S + T/z)/(-T/z) = \hat{u}/\hat{t}$ was used. From the information given in Table I and Table II, we find the following explicit expression for $\Delta\hat{\sigma}_{ag \rightarrow c}$ taking $N = 3$,

$$\Delta\hat{\sigma}_{ag \rightarrow c} = \delta_{ac} \left\{ 2 \left(1 - \frac{\hat{s}\hat{u}}{\hat{t}^2} \right) \left[\frac{9}{16} + \frac{1}{8} \left(1 + \frac{\hat{u}}{\hat{t}} \right) \right] \right. \\ \left. + \frac{4}{9} \left(\frac{-\hat{u}}{\hat{s}} + \frac{\hat{s}}{-\hat{u}} \right) \left[\frac{63}{128} - \frac{1}{64} \left(1 + \frac{\hat{u}}{\hat{t}} \right) \right] \right. \\ \left. + \left(\frac{\hat{s}}{\hat{t}} + \frac{\hat{u}}{\hat{t}} \right) \left[\frac{9}{16} + \frac{1}{8} \left(1 + \frac{\hat{u}}{\hat{t}} \right) \right] \right. \\ \left. + \left[\frac{9}{32} \left(\frac{-\hat{u}}{\hat{s}} - \frac{\hat{s}}{-\hat{u}} \right) \right] + \left[\frac{9}{16} \left(\frac{\hat{s}}{\hat{t}} - \frac{\hat{u}}{\hat{t}} \right) \right] \right\} . \quad (76a)$$

For quark-quark (or antiquark) scattering, the color factors of individual subprocess depend on quark or antiquark, as shown in Table II. For parton a a quark (corresponding to a polarized proton beam), we have

$$\Delta\hat{\sigma}_{qq' \rightarrow q} = \frac{4}{9} \left(\frac{\hat{s}^2 + \hat{u}^2}{\hat{t}^2} \right) \left[\frac{21}{64} + \frac{1}{8} \left(1 + \frac{\hat{u}}{\hat{t}} \right) \right]$$

$$\begin{aligned}
\Delta\hat{\sigma}_{q\bar{q}'\rightarrow q} &= \frac{4}{9} \left(\frac{\hat{s}^2 + \hat{u}^2}{\hat{t}^2} \right) \left[\frac{51}{64} + \frac{1}{8} \left(1 + \frac{\hat{u}}{\hat{t}} \right) \right] \\
\Delta\hat{\sigma}_{qq'\rightarrow q'} &= \frac{4}{9} \left(\frac{\hat{s}^2 + \hat{t}^2}{\hat{u}^2} \right) \left[\frac{21}{64} - \frac{51}{64} \left(1 + \frac{\hat{u}}{\hat{t}} \right) \right] \\
\Delta\hat{\sigma}_{q\bar{q}'\rightarrow\bar{q}} &= \frac{4}{9} \left(\frac{\hat{s}^2 + \hat{t}^2}{\hat{u}^2} \right) \left[\frac{51}{64} - \frac{21}{64} \left(1 + \frac{\hat{u}}{\hat{t}} \right) \right] \\
\Delta\hat{\sigma}_{qq\rightarrow q} &= \frac{-8}{27} \left(\frac{\hat{s}^2}{\hat{u}\hat{t}} \right) \left[\frac{10}{8} + \frac{1}{8} \left(1 + \frac{\hat{u}}{\hat{t}} \right) \right] \\
\Delta\hat{\sigma}_{q\bar{q}\rightarrow q'} &= \frac{4}{9} \left(\frac{\hat{t}^2 + \hat{u}^2}{\hat{s}^2} \right) \left[-\frac{1}{8} - \frac{51}{64} \left(1 + \frac{\hat{u}}{\hat{t}} \right) \right] \\
\Delta\hat{\sigma}_{q\bar{q}\rightarrow\bar{q}'} &= \frac{4}{9} \left(\frac{\hat{t}^2 + \hat{u}^2}{\hat{s}^2} \right) \left[-\frac{1}{8} - \frac{21}{64} \left(1 + \frac{\hat{u}}{\hat{t}} \right) \right] . \tag{76b}
\end{aligned}$$

For a polarized antiproton beam, similar formulas for $\Delta\hat{\sigma}_{\bar{q}b\rightarrow c}$ can be derived from Table II. From Eqs. (33) and (76), we see that the underlying partonic cross sections for spin-dependent and spin-averaged cases are similar, other than the factors in square brackets.

3. Comparison with the Fermilab Data

Because of limited phase space, most of the Fermilab data in Ref. [4] were collected at relatively small values of transverse momenta, ranging up to 4 GeV for π^0 in the central region (where A_N is small), and up to only 1.5 GeV for π^\pm, π^0 in the forward region, where A_N is large. In general, a transverse momentum of even 2 GeV is considered too small to apply perturbative QCD reliably to single-particle inclusive cross sections, because of their steep dependence on ℓ_T . This strong dependence makes the cross sections sensitive to higher-twist effects not associated directly with spin, such as intrinsic transverse momentum, hadronic scales, and, of course, yet higher powers in $1/\ell_T$. One consequence of these effects is to regularize the cross section at $\ell_T = 0$. For the asymmetry, however, the strongest power dependence on $1/\ell_T$ cancels in the ratio of the spin-dependent and spin-averaged cross sections, leaving at most λ/ℓ_T in A_N . In fact, as we will show below, A_N does not behave numerically even as steeply as $1/\ell_T$ in most of the range where the data were collected. This suggests that our calculation for A_N is perturbatively stable and may be meaningfully compared with the data.

For simplicity in our numerical estimates, we employed the following simple parametrizations, without scaling violation, for twist-two parton distributions [10],

$$xu_v(x) = \frac{2}{B(0.5, 4)} x^{0.5} (1-x)^3 , \tag{77a}$$

$$xd_v(x) = \frac{1}{B(0.5, 4.5)} x^{0.5} (1-x)^{3.5} , \tag{77b}$$

$$xS(x) = 8 \left[\frac{1}{2} - 2 \frac{B(1.5, 4)}{B(0.5, 4)} - \frac{B(1.5, 4.5)}{B(0.5, 4.5)} \right] (1-x)^7 , \tag{77c}$$

$$xG(x) = 3 (1-x)^5 . \tag{77d}$$

Here, $B(x, y)$ is the beta function. For pion fragmentation functions, we rely on Ref. [40]. Using the simplified parton distributions of Eqs. (77) in the spin-averaged cross section, and in the model for the twist-three distribution given by Eq. (71), we evaluated A_N as the ratio of the spin-dependent cross section in Eq. (74) to the spin-averaged cross section, Eq. (33).

In Fig. 20, along with experimental data from Ref. [4], we have plotted our calculated A_N for π^+ and π^- production in the scattering of a polarized antiproton beam on an unpolarized proton target. Similarly, in Fig. 21, we plot the asymmetries with a polarized proton beam. In Fig. 22, we compare theory and experiment in the asymmetries for π^0 production with a polarized antiproton beam and a polarized proton beam. The data presented in Figs. 20, 21 and 22 are averaged over the range of transverse momenta, up to 1.5 GeV. All of the calculations in these figures, however, were carried out at $\ell_T \sim 4$ GeV, with a normalization constant $\lambda = 0.080$ GeV, adjusted to give a rough match to the data.³ We will come back to the choice of ℓ_T in a moment. This limitation notwithstanding, fixing the single overall normalization constant, λ , is enough to give theoretical predictions that are consistent with the shapes and relative signs and normalizations of all the experimental data.

Now let us consider to the question of how to best to choose ℓ_T for the comparison with the data. Given the naive expectation that $A_N \sim 1/\ell_T$, the extracted value of λ might be expected to depend strongly on the value of ℓ_T at which we evaluate the asymmetries. Surprisingly, however, the perturbative prediction for the asymmetries in this momentum region is not very sensitive the precise value of ℓ_T . Thus, in Figs. 23, 24, and 25, we present the same asymmetries as in the foregoing three figures, now evaluated at $\ell_T = 1.5$ GeV. For this value, we find a good match to the data by choosing $\lambda = 0.070$ GeV, not too different from the value found at $\ell_T = 4$ GeV. Clearly, the normalizations and shapes of the asymmetries at $\ell_T = 4$ GeV and $\ell_T = 1.5$ GeV are very similar, with an only slightly different normalization factor. We consider this stability very encouraging. Such consistency is strong evidence that the twist-three formalism of perturbative QCD can be applied to single transverse-spin asymmetries at moderate transverse momenta. We will give a further discussion of this point in the next section.

We close this section with a few comments on the consequences of our model of T_F (Eqs. (71) and (72), with $\lambda \sim 0.080$ GeV) for single-spin asymmetries in direct photon production. Compared to the ansatz for T_F proposed in Ref. [10], the two main differences are, first, the relative minus sign between the down and up quark matrix elements, and, second, a decrease in the overall normalization λ , below 100 MeV. Both of these features are suggested by comparison to the data for pion production, which is only now possible. The effects of the both changes would be to reduce the cross section estimates given in Ref. [10], although the second is more important than the first, because the down quark's charge is small. In any case, the data [28] which limit the direct photon asymmetry is at low x_F , where either model predicts a small effect.

³For the purpose of this comparison, we neglect correlations between x_F and ℓ_T in the data.

V. SUMMARY AND DISCUSSION

In this section, we summarize and interpret the main features of our results and provide a few thoughts on future development on this subject.

We have presented a calculation of single transverse-spin asymmetries, A_N , for hadronic pion production at large x_F . This calculation was based on a “valence quark-soft gluon” approximation. In this approximation, we kept only those contributions to A_N proportional to the derivative of the twist-3 quark gluon correlation function, $(\partial/\partial x)T_{Fa}^{(V)}(x, x)$, where a denotes a valence quark flavor, and where the equal arguments in T_F imply zero gluon momentum fraction. Our results for spin-dependent single-spin cross sections are given in Eq. (74). The ratio of the spin-dependent cross section in Eq. (74) and the spin-averaged cross section in Eq. (33) defines A_N for hadronic pion production. The spin-dependent cross section, Eq. (74) has two types of contributions: quark-gluon and quark-quark (or antiquark), which are given by $\Delta\hat{\sigma}_{ag \rightarrow c}$ in Eq. (76a) and $\Delta\hat{\sigma}_{ab \rightarrow c}$ in Eq. (76b), respectively. All of these calculations are strictly leading order; we anticipate that a large part of higher order corrections will cancel in the asymmetry. Our model for the twist-3 matrix element T_F is given in Eqs. (71) and (72). We have not investigated the evolution properties of these matrix elements here. We expect this to be an interesting subject, but we do not anticipate that evolution will require qualitative changes in our conclusions.

Single transverse-spin asymmetries are a twist-three effect in QCD perturbation theory. After taking the ratio of Eqs. (74) and (33), the asymmetry has following schematic dependence on kinematic variables in the large x_F region,

$$A_N \sim \lambda \frac{\ell_T}{(-U)} \left[1 + O\left(\frac{U}{T}\right) \right] \frac{1}{1 - x_F}, \quad (78)$$

where the invariants, U and T are defined in Eq. (3). In Eq. (78), the prefactor $\ell_T/(-U)$ comes directly from the factor $\epsilon^{\ell_{ST}n\bar{n}}/(-\hat{u})$ in the spin-dependent cross section in Eq. (74). The combination $[1 + O(U/T)]$ is left over from the partonic cross sections in Eq. (76), after the cancelation of the dominant $1/\hat{t}^2$ dependence in the ratio. The normalization parameter λ comes from our model of the twist-three correlation functions, $T_F^{(V)}(x, x)$ in Eq. (71). Finally, the factor $1/(1 - x_F)$ for x_F large is associated with $(\partial/\partial x)T_F^{(V)}(x, x)$ in Eq. (74). The approximate $1/(1 - x_F)$ behavior in the ratio of the derivative of the twist-three correlation function to the corresponding twist-two parton distribution is the dominant feature of the twist-three asymmetry, and is responsible for the observed growth of A_N in the large- x_F region.

The factors $\ell_T/(-U)$ and $\ell_T/(-T)$ in Eq. (78) reflect the twist-three nature of the asymmetry, A_N . Combining Eqs. (3) and (4), we express the invariants, U and T , in terms of x_F and ℓ_T ,

$$U = -\frac{S}{2} \left[\sqrt{x_F^2 + x_T^2} + x_F \right] \quad (79a)$$

$$T = -\frac{S}{2} \left[\sqrt{x_F^2 + x_T^2} - x_F \right]. \quad (79b)$$

When $x_F = 0$, both U and T are equal to $\ell_T \sqrt{S}$. From Eq. (78), we conclude that the asymmetry at $x_F = 0$ should have a very mild, probably linear dependence on the pion’s

transverse momentum (A_N must vanish at $\ell_T = 0$). Our analytical results in Eq. (74), however, are not accurate for the asymmetry near $x_F = 0$, because of the large x_F approximation used in our calculations. But, from the general structure of the asymmetry, we believe that weak transverse momentum dependence at $x_F = 0$ for A_N should be a more general conclusion.

If $x_F \gg x_T$, the invariants U and T in Eq. (79) have the following approximate dependence on ℓ_T and x_F ,

$$U \rightarrow -x_F S , \quad (80a)$$

$$T \rightarrow -\frac{\ell_T^2}{x_F} . \quad (80b)$$

Consequently, in the large x_F region, the asymmetry, A_N , will have two typical contributions, λ/ℓ_T and $\lambda\ell_T/S$, respectively. If the λ/ℓ_T contribution dominates, perturbative QCD calculations of the asymmetry may be relatively sensitive to nonperturbative effects, because of its singular behavior at $\ell_T = 0$. On the other hand, QCD perturbation theory may provide a reliable calculation of the asymmetries when the $\lambda\ell_T/S$ term is relatively important. In Fig. 26, we plot the transverse momentum dependence of the asymmetry at $x_F = 0.4$, where most data were collected. The asymmetries for both π^+ and π^- have a quite weak dependence on pion's transverse momentum for $\ell_T > 2$ GeV. This suggests that perturbative calculations for the asymmetries are reliable for a wide range of the experimental kinematics.

The remarkable feature of mild transverse momentum dependence, shown in Fig. 26, can be easily traced to Eq. (76). For the quark-gluon subprocess, once the dominant $1/\hat{t}^2$ dependence has canceled in the asymmetry, the coefficient of \hat{u}/\hat{t} is much smaller than the corresponding constant term. Similarly, for quark-quark and antiquark subprocess, the coefficient of \hat{u}/\hat{t} is also much smaller than the constant term, except for terms proportional to $1/\hat{u}^2$ and $1/\hat{s}^2$. The latter, however, are suppressed by \hat{t}^2/\hat{s}^2 relative to the leading terms in the forward region. In summary, the small coefficients for \hat{u}/\hat{t} terms assure that the $\ell_T/(-T)$ dependence in Eq. (78) does not dominate the $\ell_T/(-U)$ dependence. We verify this conclusion by plotting the fractional contributions to the π^+ asymmetry from $1/(-U)$ term and $1/(-T)$ term, respectively, as a function of pion's transverse momentum in Fig. 27. It is evident that contribution from $1/(-U)$ term is comparable with $1/(-T)$ term for the region of our interest.

If $x_F \rightarrow 1$, or $U/T \sim x_F^2 S/\ell_T^2 \gg 1$, the asymmetry will be eventually dominated by the λ/ℓ_T terms. Therefore, the asymmetry will scale with $1/\ell_T$ in this region. For the kinematics of the Fermilab data, this scaling region is not yet reached. In Fig. 26, the steep increase of the asymmetries for $\ell_T < 2$ GeV indicates the dominance of the λ/ℓ_T contribution, and probably signals that the perturbative calculations are relatively less reliable if ℓ_T is much less than 2 GeV. The slight increase when $\ell_T \rightarrow 6$ GeV signals an effect of the edge of phase space. Clearly, the high energies of the polarized RHIC proton beam would make it possible to check these predictions. In Fig. 28, we show the ℓ_T -dependence of A_N for $x_F = 0.4$ at $\sqrt{S} = 200$ GeV. Compared to Fig. 26 at Fermilab energies, the ℓ_T/U term is relatively suppressed, and the model predicts a steeper ℓ_T -dependence and, in general, a smaller, but still substantial, asymmetry. Fig. 29 shows the asymmetry as a function of x_F at $\ell_T = 4$ GeV. These are examples only; the model can be used to predict A_N over any kinematic range that is experimentally convenient, so long as it is in the forward region.

In summary, we have calculated the single transverse-spin asymmetry for hadronic pion production in perturbative QCD. With only one normalization parameter λ and a relative sign of polarized twist-3 valence quark distributions, our numerical results are consistent with Fermilab data on the asymmetry for both the sign and shape, as well as relative normalizations. In addition, we demonstrated that perturbative calculation of the asymmetries is applicable even for pion momenta as small as a few GeV. This conclusion is very encouraging for future applications of perturbative QCD beyond the leading twist. Our method can be easily generalized to calculate the single transverse-spin asymmetries for inclusive production of other particles. The planned polarized beam at RHIC affords an exciting opportunity to test these, and related ideas on the spin structure of the nucleon.

ACKNOWLEDGMENTS

We thank Aki Yokosawa for helpful communications regarding the Fermilab data, and R.L. Jaffe and P. Ratcliffe for useful conversations. This work was supported in part by the U.S. Department of Energy under Grant Nos. DE-FG02-87ER40731 and DE-AC02-98CH10886 and by the National Science Foundation, under grant PHY9722101.

APPENDIX

In this appendix, we identify twist-3 distributions and fragmentation functions that can contribute to the sums in the collinear expansion, Eq. (17). The factorization in (17) enables us to apply parity and time-reversal (PT) invariance to hadron-hadron scattering in a manner similar to their classic application to inclusive DIS, reviewed in Sec. II A. Thus, it will be natural to study the symmetry properties of possible matrix elements.

We will identify terms of the type discussed in connection with Eq. (29), that is, with integrals over two quark momentum fractions, x_1 and x_2 . Furthermore, we require that x_1 be set equal to x_2 by a “gluonic” pole at $x_1 = x_2$ in the hard scattering (see Eq. (47)), in accordance with our valence quark-soft gluon approximation. Let us concentrate first on parton distributions, and return at the end to fragmentation functions.

Twist-3 Distributions

As mentioned in Sec. II C, the derivation of terms in Eq. (17) involving quarks requires a Fierz projection of the Dirac indices linking the distribution or fragmentation function and the hard scattering. A schematic illustration was given in Fig. 7. The collinear expansion then isolates twist-three fermion matrix elements with two quark fields and either a covariant derivative or a field strength. It will be convenient to start by discussing the expectation values of combinations of these fields in position space. We thus introduce

$$D_\Gamma^i(y_1, y_2, s) = \langle P, s | \bar{\psi}(0) \Gamma D^i(y_2) \psi(y_1) | P, s \rangle \quad (81)$$

$$F_\Gamma^i(y_1, y_2, s) = \langle P, s | \bar{\psi}(0) \Gamma n_\mu F^{i\mu}(y_2) \psi(y_1) | P, s \rangle, \quad (82)$$

with Γ a Dirac matrix. We define $D^i \equiv i\partial^i - gA^i$, and we adopt the kinematics and notation of Sec. II A; in particular, n^μ is defined in Eq. (2). In these matrix elements, the index i

is assumed to be transverse. This alone is enough to make the matrix element twist-3; the Dirac projection must not raise the twist further. The relevant terms in the Fierz projection between the distribution for a hadron of momentum $P^\mu = \bar{n}^\mu \sqrt{S/2}$ and the hard scattering are then given by

$$\begin{aligned}\delta_{aa'}\delta_{bb'} &= \frac{1}{4}(\gamma \cdot n)_{ab}(\gamma \cdot \bar{n})_{b'a'} + \frac{1}{4}(\gamma \cdot n\gamma_5)_{ab}(\gamma_5\gamma \cdot \bar{n})_{b'a'} \\ &+ \frac{1}{4} \sum_{\beta} ((n\sigma)_{\beta})_{ab} ((\bar{n}\sigma)^{\beta})_{b'a'} + \dots,\end{aligned}\quad (83)$$

where omitted terms raise the twist, and where we define

$$(n\sigma)^{\beta} \equiv n_{\mu}\sigma^{\mu\beta}. \quad (84)$$

For an opposite-moving hadron, with momentum $P'^\mu = n^\mu \sqrt{S/2}$, we exchange the roles of n^μ and \bar{n}^μ . The matrices above have the properties

$$\Gamma = \gamma^0 \Gamma^{\dagger} \gamma^0, \quad (85)$$

$$\Gamma = \delta_{\Gamma} (\mathcal{T}\Gamma^*\mathcal{T})^{\dagger}, \quad (86)$$

with $\delta_{\Gamma} = \pm 1$, where $\mathcal{T} \equiv i\gamma^1\gamma^3 = \mathcal{T}^{-1}$ is a time-reversal matrix that acts as

$$\mathcal{T}(\gamma^{\mu})^* \mathcal{T} = \gamma_{\mu}. \quad (87)$$

Specifically, for the vector, axial-vector and tensor cases we have

$$n \cdot \gamma : \quad \delta_{n \cdot \gamma} = 1 \quad (88)$$

$$n \cdot \gamma\gamma_5 : \quad \delta_{n \cdot \gamma\gamma_5} = -1 \quad (89)$$

$$(n\sigma)^{\nu} : \quad \delta_{(n\sigma)^{\nu}} = -1. \quad (90)$$

From the expectation values F_{Γ}^i and D_{Γ}^i we define parton distributions by Fourier transforms with respect to light-cone momenta, and if desired transverse momenta as well,

$$t_{\Gamma}^{(D)i}(x_1, \mathbf{k}_1, x_2, \mathbf{k}_2, s) = \int dy_1 dy_2 e^{ik_1 \cdot y_1 + i(k_2 - k_1) \cdot y_2} D_{\Gamma}^i(y_1, y_2, s), \quad (91)$$

$$t_{\Gamma}^{(F)i}(x_1, \mathbf{k}_1, x_2, \mathbf{k}_2, s) = \int dy_1 dy_2 e^{ik_1 \cdot y_1 + i(k_2 - k_1) \cdot y_2} F_{\Gamma}^i(y_1, y_2, s), \quad (92)$$

where we define $dy_i \equiv dy^- d^2\mathbf{y}$, with \mathbf{y} a two-dimensional transverse vector, and $k_i \cdot y \equiv x_i p y^- - \mathbf{k} \cdot \mathbf{y}$. In the following, we study constraints on spin-dependence that follow from the reality and symmetry properties of these matrix elements in QCD. This will enable us to identify the relevant contributions to the sums in Eq. (17).

Reality and Symmetry

The reality properties of the matrix elements (81) and (82) are conveniently expressed as

$$\left[D_\Gamma^i(-y_1, -y_2, s) \right]^* = D_\Gamma^i(y_1, y_1 - y_2, s), \quad (93)$$

$$\left[F_\Gamma^i(-y_1, -y_2, s) \right]^* = F_\Gamma^i(y_1, y_1 - y_2, s), \quad (94)$$

which relate, of course, expectation values with the same spins. Invariance under time reversal and parity, on the other hand imply that

$$D_\Gamma^i(y_1, y_2, s) = \delta_\Gamma D_\Gamma^i(y_1, y_1 - y_2, -s), \quad (95)$$

$$F_\Gamma^i(y_1, y_2, s) = -\delta_\Gamma F_\Gamma^i(y_1, y_1 - y_2, -s), \quad (96)$$

in which spins are reversed.

Relations for parton distributions $t_\Gamma^{(D)i}$ and $t_\Gamma^{(F)i}$ are easy to derive by inserting the reality and symmetry relations into the Fourier transforms of Eqs. (91) and (92), and changing integration variables. Because in this paper we are concentrating on the collinear expansion, with convolutions in light-cone momenta only, we shall suppress transverse momenta in the arguments of the distributions, and exhibit only the momentum fraction variables x_i in the following formulas. Relations for transverse-momentum distributions are found by simply reinserting the \mathbf{k}_i arguments, alongside the corresponding momentum fractions. With this understood, the reality conditions give

$$\left[t_\Gamma^{(D)i}(x_1, x_2, s) \right]^* = t_\Gamma^{(D)i}(x_2, x_1, s), \quad (97)$$

$$\left[t_\Gamma^{(F)i}(x_1, x_2, s) \right]^* = t_\Gamma^{(F)i}(x_2, x_1, s), \quad (98)$$

in which we note that the momentum arguments are exchanged. Referring to Eqs. (88-90) above, we see that the even parts of the twist-3 distributions are real, the odd parts imaginary.

Similarly, from PT invariance, we find

$$t_\Gamma^{(D)i}(x_1, x_2, s) = \delta_\Gamma t_\Gamma^{(D)i}(x_2, x_1, -s), \quad (99)$$

$$t_\Gamma^{(F)i}(x_1, x_2, s) = -\delta_\Gamma t_\Gamma^{(F)i}(x_2, x_1, -s), \quad (100)$$

with δ_Γ defined in Eq. (86). Note the extra minus sign in the second case, which reflects the PT properties of the field strength tensor.

From Eqs. (97-100), we can derive the constraints on the spin-averaged,

$$\langle t_\Gamma^{(O)i} \rangle(x_1, x_2) \equiv \frac{1}{2} \left[t_\Gamma^{(O)i}(x_1, x_2, s) + t_\Gamma^{(O)i}(x_1, x_2, -s) \right] \quad (101)$$

and spin-dependent

$$\Delta t_\Gamma^{(O)i}(x_1, x_2) \equiv \frac{1}{2} \left[t_\Gamma^{(O)i}(x_1, x_2, s) - t_\Gamma^{(O)i}(x_1, x_2, -s) \right] \quad (102)$$

distributions for each choice of operator $O = D, F$ and Dirac structure Γ . Specifically, the spin-dependent distributions $\Delta t_{n\cdot\gamma}^{(D)i}$, $\Delta t_{n\cdot\gamma\gamma_5}^{(F)i}$ and $\Delta t_{(n\sigma)^j}^{(F)i}$ and the spin-averaged distributions $\langle t_{n\cdot\gamma\gamma_5}^{(D)i} \rangle$, $\langle t_{(n\sigma)^j}^{(D)i} \rangle$ and $\langle t_{n\cdot\gamma}^{(F)i} \rangle$ are imaginary and vanish at $x_1 = x_2$. They therefore cannot be associated with gluon poles in Eq. (17), and are nonleading in the valence quark-soft gluon approximation introduced in Sec. II B.

Leading Terms at Twist-3

The remaining distributions are real and nonzero at $x_1 = x_2$ in general. For the first sum in Eq. (17), we need a real, chiral-even, spin-dependent parton distribution. The only one is $\Delta t_{n\cdot\gamma}^{(F)i}(x_1, x_2)$, which is equal, up to a constant, to $T_F^{(V)}$, Eq. (25),

$$\Delta t_{n\cdot\gamma}^{(F)i}(x_1, x_2) = -4\pi\epsilon^{n\bar{n}is} T_F^{(V)}(x_1, x_2), \quad (103)$$

where the tensor structure follows from parity invariance applied to the matrix element.

For the second sum in Eq. (17), we need a chiral-odd *spin-averaged* distribution, to give a nonzero trace in the hard-scattering amplitude when paired with the transversity distribution [22],

$$\delta q(x) = \int \frac{dy^-}{2\pi} e^{ixP^+y^-} \langle P, s | \bar{\psi}(0) \frac{i}{2}(n\sigma)^i s_i \gamma_5 \psi(y^- n) | P, s \rangle. \quad (104)$$

Here again there is only a single contribution, $\langle t_{(\bar{n}\sigma)^j}^{(F)i} \rangle(x_1, x_2)$. Parity invariance implies that $\langle t_{(\bar{n}\sigma)^j}^{(F)i} \rangle(x_1, x_2)$ is of the form

$$\langle t_{(\bar{n}\sigma)^j}^{(F)i} \rangle(x_1, x_2) = 4\pi \frac{\delta_{ij}}{2} T_F^{(\sigma)}(x_1, x_2), \quad (105)$$

where the scalar distribution $T_F^{(\sigma)}$ is defined by analogy to $T_F^{(V)}$, Eq. (25),

$$\begin{aligned} T_F^{(\sigma)}(x_1, x_2) &= \int \frac{dy_1^+ dy_2^+}{4\pi} e^{ix_1 P'^- y_1^+ + i(x_2 - x_1) P'^- y_2^+} \\ &\quad \times \frac{1}{2} \sum_{s'} \langle P', s' | \bar{\psi}(0) (\bar{n}\sigma)_j \bar{n}_\rho F^{j\rho}(y_2^+) \psi(y_1^+) | P', s' \rangle. \end{aligned} \quad (106)$$

In these expressions we have taken P'^μ in the minus- z direction, in accordance with the kinematics of the unpolarized hadron in Sec. II A. In Ref. [10] the possibility of such a term was noted.

Fragmentation at Twist-3

Turning to the third term in Eq. (17), we must deal with twist-3 chiral-even fragmentation functions, which are transforms of matrix elements of the general form

$$\bar{d}^{(\sigma)}(y_1, y_2, \ell) = \sum_X \text{Tr} \left[(n_\ell \sigma)_i \langle 0 | \bar{\psi}(0) | \ell, X \rangle \langle \ell, X | D^i(y_2) \psi(y_1) | 0 \rangle \right] \quad (107)$$

$$\bar{f}^{(\sigma)}(y_1, y_2, \ell) = \sum_X \text{Tr} \left[(n_\ell \sigma)_i \langle 0 | \bar{\psi}(0) | \ell, X \rangle \langle \ell, X | n_{\ell\mu} F^{\mu i}(y_2) \psi(y_1) | 0 \rangle \right], \quad (108)$$

with the sum over inclusive final (out) states $|X, \ell\rangle$, where ℓ is the momentum of the observed particle. The vector n_ℓ^μ is defined by analogy to n^μ in Eq. (2), as a lightlike velocity vector

in the direction opposite to $\bar{n}_\ell \equiv \ell^\mu/\ell_0$. The trace is over Dirac indices. There is no analog of the spin variable in this case, although extensions to production of polarized particles [3] should be straightforward. We have used the constraints of parity in forming scalar fragmentation functions, depending on two momentum fractions. In momentum space they are

$$d^{(\sigma)}(z_1, z_2) = \int \frac{dy_1 dy_2}{4\pi} e^{-i\ell \cdot ny_1/z_1 - i\ell \cdot ny_2(1/z_2 - 1/z_1)} \bar{d}^{(\sigma)}(y_1, y_2, \ell) \quad (109)$$

$$f^{(\sigma)}(z_1, z_2) = \int \frac{dy_1 dy_2}{4\pi} e^{-i\ell \cdot ny_1/z_1 - i\ell \cdot ny_2(1/z_2 - 1/z_1)} \bar{f}^{(\sigma)}(y_1, y_2, \ell). \quad (110)$$

The constraints of reality are different for these fragmentation functions than for the distributions, because the sums over states in Eqs (107) and (108) are incomplete. We find that

$$\bar{d}^{(\sigma)*}(-y_1, -y_2, \ell) = \sum_X \text{Tr} [(\bar{n}_\ell \sigma)_i \langle 0 | \bar{\psi}(0) D^i(y_1 - y_2) | \ell, X \rangle \langle \ell, X | \psi(y_1) | 0 \rangle] \quad (111)$$

$$\bar{f}^{(\sigma)*}(-y_1, -y_2, \ell) = \sum_X \text{Tr} [(\bar{n}_\ell \sigma)_i \langle 0 | \bar{\psi}(0) \bar{n}_\mu F^{\mu i}(y_1 - y_2) | \ell, X \rangle \langle \ell, X | \psi(y_1) | 0 \rangle]. \quad (112)$$

As Collins has emphasized [17], time-reversal does not constrain fragmentation functions in the same manner as distributions, because T reverses the roles of in and out states. To the extent that a sum over in and out states is the same in these functions, symmetry under PT would imply that $\bar{d}^{(\sigma)}$ is purely imaginary, while $\bar{f}^{(\sigma)}$ is real. These properties can, however, be modified by phases associated with final state interactions. Indeed, this is the mechanism by which Artru *et al.* [19] derive single-spin asymmetries starting from a model for fragmentation functions with intrinsic transverse momenta. Such functions can be thought of as extensions of $\bar{d}^{(\sigma)}$, finite distances from the light cone. Following the procedure of Sec. III above, we can derive hard-scattering coefficients for either function. We reserve this for future investigation.

REFERENCES

- [1] J. Ashman et al., Phys. Lett. **B206**, 364 (1988).
- [2] For a recent review, see, for example, R.L. Jaffe, in the proceedings of *Ettore Majorana International School of Nucleon Structure: The Spin Structure of the Nucleon*, Erice, Italy, 3-10 Aug 1995, hep-ph/9602236.
- [3] G. Bunce et al., Phys. Rev. Lett. **36**, 1113 (1976); K. Heller et al., Phys. Lett. **B68**, 480 (1977); S.A. Gourlay et al., Phys. Rev. Lett. **56**, 2244 (1986).
- [4] D.L. Adams et al., Phys. Lett. **B261**, 201 (1991); **B264**, 462 (1991); A. Bravar et al., Phys. Rev. Lett. **77**, 2626 (1996).
- [5] J.F. Owens, Rev. Mod. Phys. **59**, 465 (1987).
- [6] G.L. Kane, J. Pumplin and W. Repko, Phys. Rev. Lett. **41**, 1689 (1978).
- [7] A.V. Efremov and O.V. Teryaev, Sov. J. Nucl. Phys. **36**, 140 (1982) [Yad. Fiz. **36**, 242, (1982)].
- [8] A.V. Efremov and O.V. Teryaev, Phys. Lett. **150B**, 383 (1985); Sov. J. Nucl. Phys. **36**, 557 (1982); **39**, 962 (1984)[Yad. Fiz. **36**, 950 (1982); **39**, 1517, (1984)].
- [9] A.V. Efremov, V. Korotkiyan and O. Teryaev, Phys. Lett. **B348**, 577 (1995).
- [10] J.W. Qiu and G. Sterman, Phys. Rev. Lett. **67**, 2264 (1991); Nucl. Phys. **B378**, 52 (1992).
- [11] J.W. Qiu and G. Sterman, in *Polarized Collider Workshop*, University Park, PA, 1990, AIP Conference Proceedings 233, ed. J.C. Collins, S.F. Heppelman, and R.W. Robinett (American Institute of Physics, New York, 1990).
- [12] M.G. Ryskin, Sov. J. Nucl. Phys. **48**, 708 (1988); D.I. D'yakanov and V.Yu. Petrov, Sov. Phys. JETP, **62**, 204 (1985).
- [13] A. Schäfer, L. Mankiewicz, P. Gornicki and S. Güllenstern, Phys. Rev. **D47**, 1 (1993); B. Ehrnsperger, A. Schäfer, W. Greiner and L. Mankiewicz, Phys. Lett. **B321**, 121 (1994).
- [14] D. Boer and P.J. Mulders, Phys. Rev. **D57**, 3057 (1998).
- [15] D. Sivers, Phys. Rev. **D41**, 83 (1990); Phys. Rev., **D43**, 261 (1991).
- [16] M. Anselmino, M. Boglione and F. Murgia, Phys. Lett. **B362**, 164 (1995).
- [17] J. Collins, Nucl. Phys. **B396**, 161 (1993); J.C. Collins, S.F. Heppelmann and G.A. Ladinsky, Nucl. Phys. **B420**, 565 (1994).
- [18] R.L. Jaffe and X.-d. Ji, Phys. Rev. Lett. **71**, 2547 (1993).
- [19] X. Artru , J. Czyzewski and H. Yabuki, Z. Phys. **C73**, 527 (1997); X. Artru and J. Czyzewski, hep-ph/9805463.
- [20] J. Huston et al., Phys. Rev. **D51**, 6139 (1995); H. Baer and M.H. Reno, Phys., Rev. **D54**, 2017 (1996); A.D. Martin, R.G. Roberts, W.J. Stirling and R.S. Thorne, hep-ph/9803445.
- [21] J.P. Ralston and D.E. Soper, Nucl. Phys. **B152**, 109 (1979).
- [22] R.L. Jaffe and X.-d. Ji, Phys. Rev. Lett. **67**, 552 (1991); Nucl. Phys. **B375**, 527 (1992); X.-d. Ji, Phys. Lett. **B284**, 137 (1992).
- [23] S.M. Troshin and N.E. Tyurin, Phys. Rev. **D52**, 3862 (1995); Phys. Rev., **D54**, 838 (1996).
- [24] C. Boros, Z.-t. Liang, T.-c. Meng, Phys. Rev. **D51**, 4867 (1995).
- [25] P.M. Nadolsky, S.M. Troshin and N.E. Tyurin, Int. J. Mod. Phys. **A9**, 2505 (1994).
- [26] C. Boros, Z.-t. Liang, T.-c. Meng and R. Rittel, J. Phys. **G24**, 75 (1998).

- [27] N. Christ and T.D. Lee, Phys. Rev. **143**, 1310 (1966).
- [28] D.L. Adams et al., Phys. Lett. **B345**, 569 (1995).
- [29] P.G. Ratcliffe, Nucl. Phys. **B264**, 493 (1986).
- [30] X.-d. Ji, Phys. Lett. **B289**, 137 (1992).
- [31] J.C. Collins, D.E. Soper and G. Sterman, in *Perturbative QCD*, ed. A.H. Mueller (World Scientific, Singapore, 1989).
- [32] J.W. Qiu and G. Sterman, Nucl. Phys. **B353**, 105 (1991).
- [33] J.W. Qiu and G. Sterman, Nucl. Phys. **B353**, 137 (1991).
- [34] R.K. Ellis, W. Furmanski and R. Petronzio, Nucl. Phys. **B207**, 1 (1982); Nucl. Phys. **B212**, 29 (1983); R.L. Jaffe, Nucl. Phys. **B229**, 205 (1983).
- [35] J.W. Qiu, Phys. Rev. **D42**, 30 (1990).
- [36] Y.L. Dokshitzer, G. Marchesini and B.R. Webber, Nucl. Phys. **B469**, 93 (1996); M. Dasgupta and B.R. Webber, Phys. Lett. **B382**, 273 (1996); Nucl. Phys. **B484**, 247 (1997).
- [37] E. Stein, M. Meyer-Hermann, L. Mankiewicz and A. Schäfer, Phys. Lett. **B376**, 177 (1996); M. Meyer-Hermann *et al.*, Phys. Lett. **B383**, 463 (1996) (E., **B393**, 487 (1997)); E. Stein, M. Maul, L. Mankiewicz and A. Schäfer, hep-ph/9803342;
- [38] M. Beneke, V.M. Braun and L. Magnea, Nucl. Phys. **B497**, 297 (1997).
- [39] J.C. Collins and D.E. Soper, Nucl. Phys. **B194**, 445 (1982).
- [40] R. Baier, J. Engles and B. Petersson, Z. Phys. **C2**, 265 (1979).

FIGURES

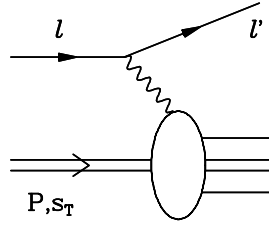


FIG. 1. Inclusive lepton-hadron deep-inelastic scattering, with the target hadron polarized transversely.

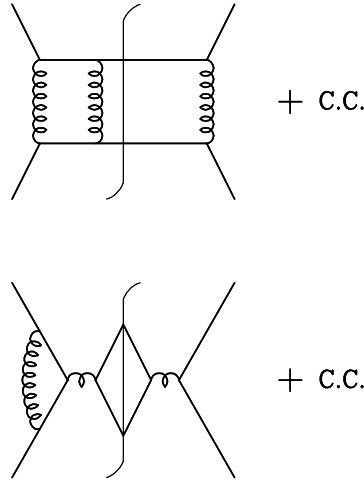


FIG. 2. Quark-quark scattering diagrams that give a nonvanishing single transverse-spin asymmetry in large- p_T reactions [6].

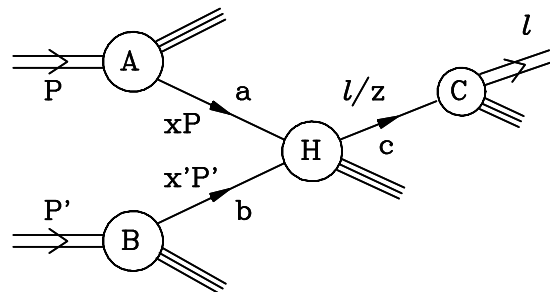


FIG. 3. Sketch of single pion production in spin-averaged hadron-hadron collisions.

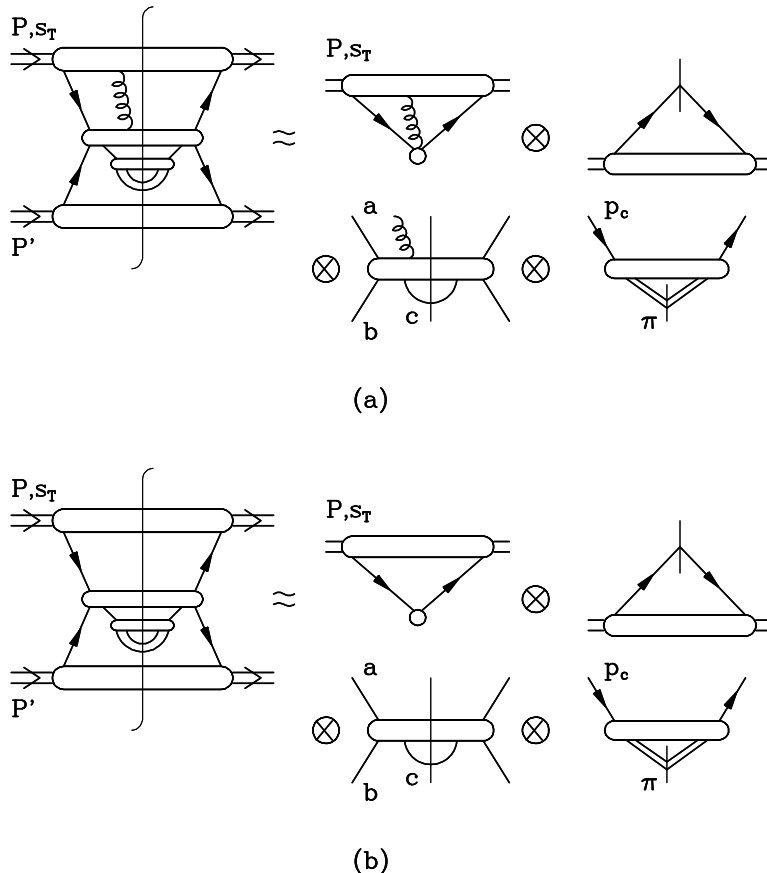


FIG. 4. Factorization of a typical forward scattering amplitude contributing to the spin-dependent cross section for hadronic pion production: (a) with chiral-even three-parton matrix element, (b) with chiral-odd transversity.

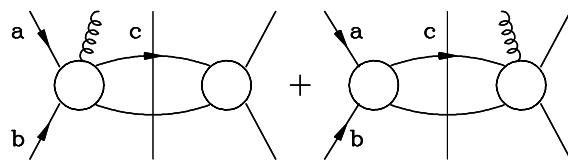


FIG. 5. General Feynman diagrams contributing to the partonic parts H in Eq. (17).

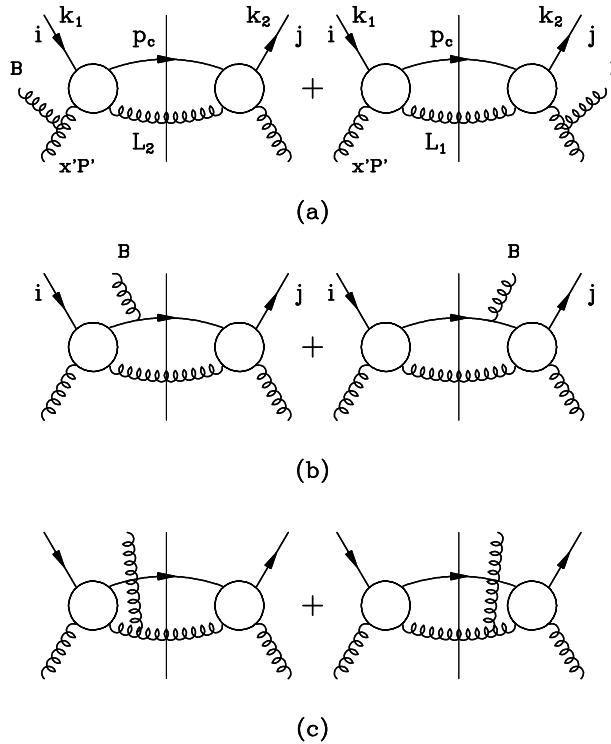


FIG. 6. Three classes of quark-gluon diagrams contributing to the spin-dependent cross section $\Delta\sigma(\vec{s}_T)$: (a) diagrams with an initial-state pole, (b) and (c) diagrams with a final-state pole. Symbols B and ij are color indices for the gluon and quarks.

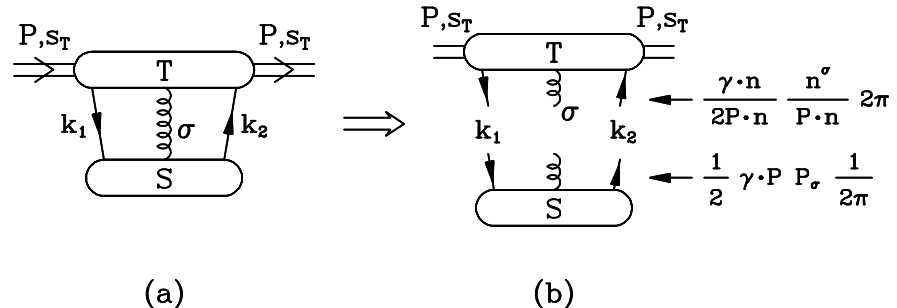


FIG. 7. General diagram that gives a leading contribution to $\Delta\sigma(\vec{s}_T)$: (a) before separation of spinor trace and Lorentz indices, (b) leading contribution after separation of spinor trace and Lorentz indices.

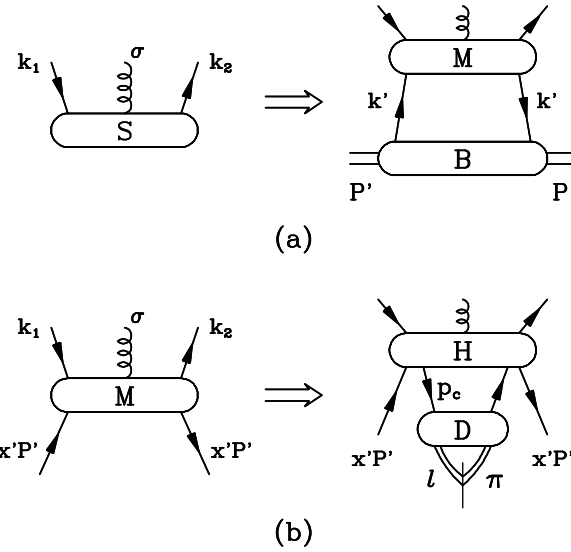


FIG. 8. Factorization of a general diagram contributing to $S_a(k_1, k_2)$ of Eq. (23): (a) separation of target hadron, (b) separation of final-state pion.

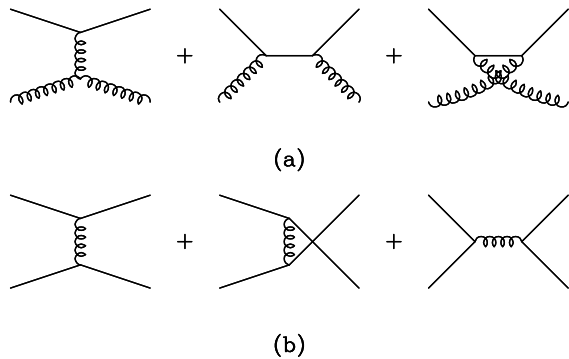


FIG. 9. Sample leading order Feynman diagrams contributing to the cross section of hadronic single pion production.

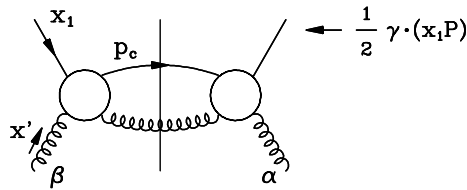


FIG. 10. Two-parton forward scattering amplitude contributing to the partonic hard part $H_{2 \rightarrow 2}(x, x', p_c)$ in Eq. (43).

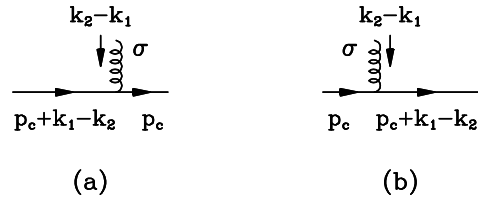


FIG. 11. Sketch for the effective diagrams giving the leading poles in Eq. (48): (a) pole to the left of the cut; (b) pole to the right of the cut.

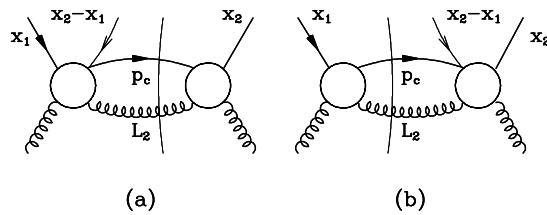


FIG. 12. Effective quark-gluon $2 \rightarrow 2$ diagrams with the thin line of momentum $(x_2 - x_1)P$ representing momentum flow that is a result of the extra final-state interaction.

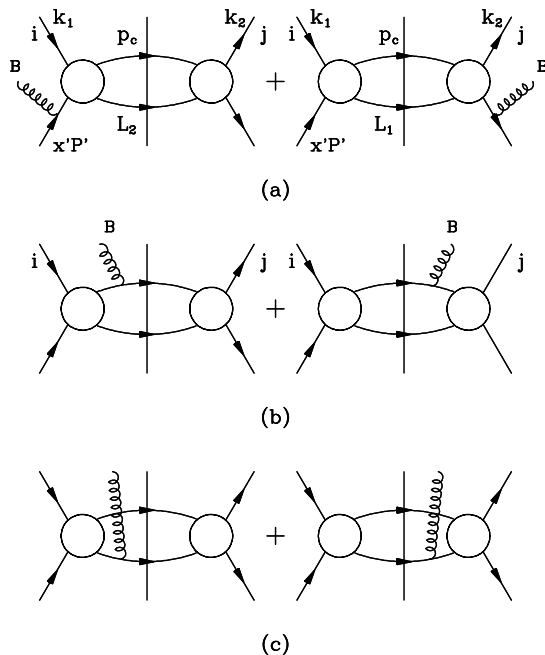


FIG. 13. Three classes of quark-quark (or antiquark) diagrams contributing to the spin-dependent cross section $\Delta\sigma(\vec{s}_T)$: (a) diagrams with an initial-state pole, (b) and (c) diagrams with a final-state pole. Symbols B and ij are color indices for the gluon and quarks.

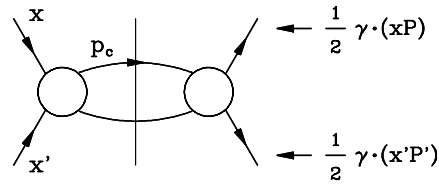


FIG. 14. Effective quark-quark (and antiquark) $2 \rightarrow 2$ diagrams contributing to the partonic hard parts, $H_{aq \rightarrow c}$.

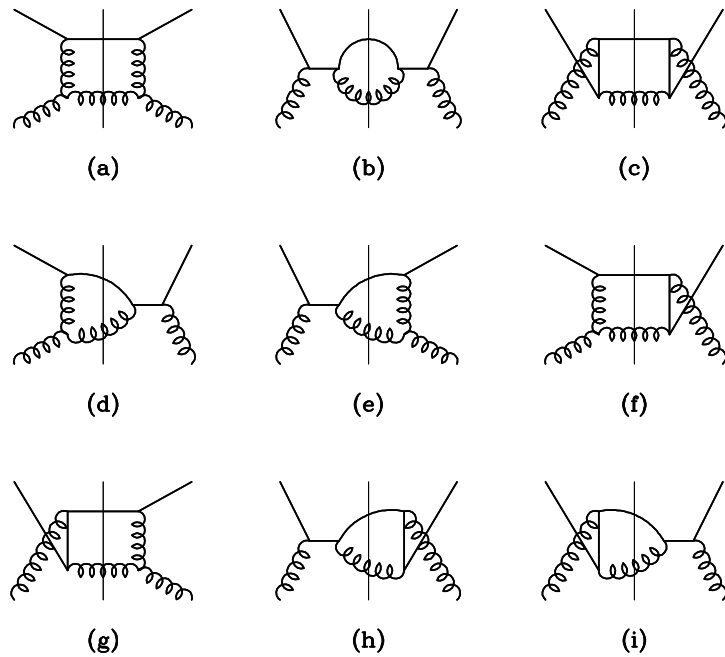


FIG. 15. All $2 \rightarrow 2$ quark-gluon diagrams contributing to partonic hard parts, $H_{ag \rightarrow c}$.

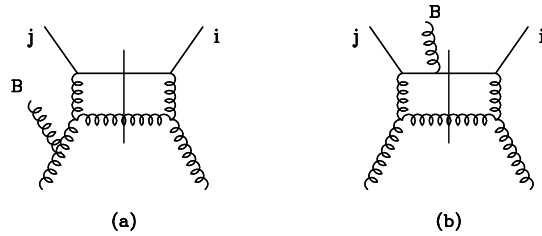


FIG. 16. Sample diagrams with initial-state and final-state interactions, used to calculate the color factors, C_g^I and C_g^F in Table I.

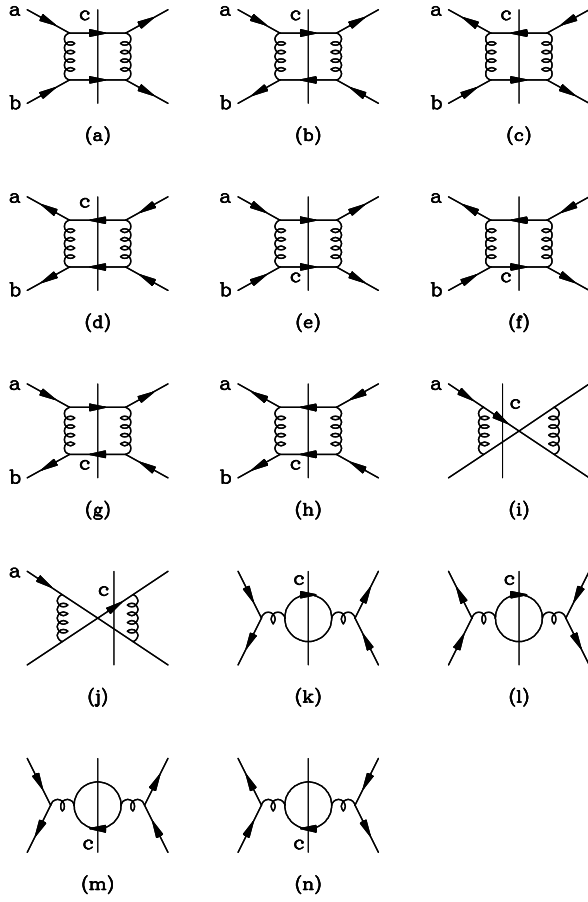


FIG. 17. All $2 \rightarrow 2$ quark-quark (and antiquark) diagrams contributing to partonic hard parts, $H_{aq \rightarrow c}$.

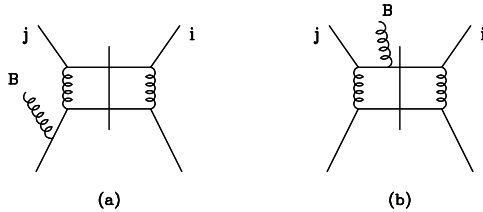


FIG. 18. Sample diagrams with initial-state and final-state interactions, used to calculate the color factors, C_q^I and C_q^F in Table II.

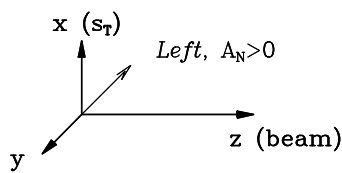


FIG. 19. Sketch for the coordinate system: the polarized beam is along the z -axis and the beam particle spin along the x -axis. Positive A_N corresponds to an excess of events in the $-y$ -direction.

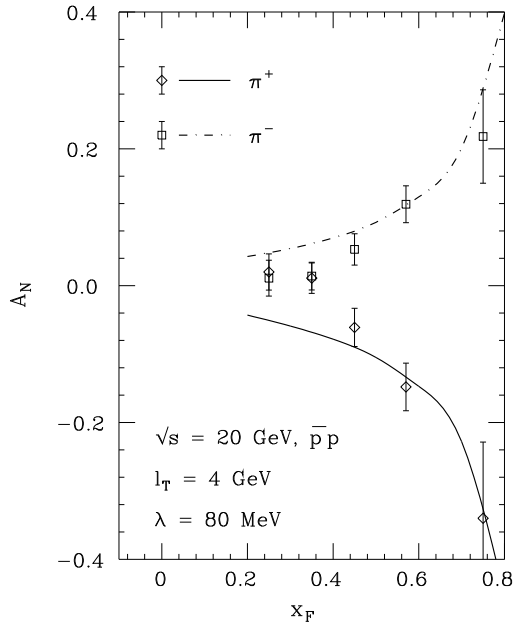


FIG. 20. Single transverse-spin asymmetry as a function of x_F for π^+ and π^- production with a polarized *antiproton* beam. Here and in the following five figures, data are from Ref. [4] at $\sqrt{S} = 20$ GeV and l_T up to 1.5 GeV. Theory curves are evaluated at transverse momentum $l_T = 4$ GeV and $\lambda = 0.080$ GeV at the same center-of-mass energy.

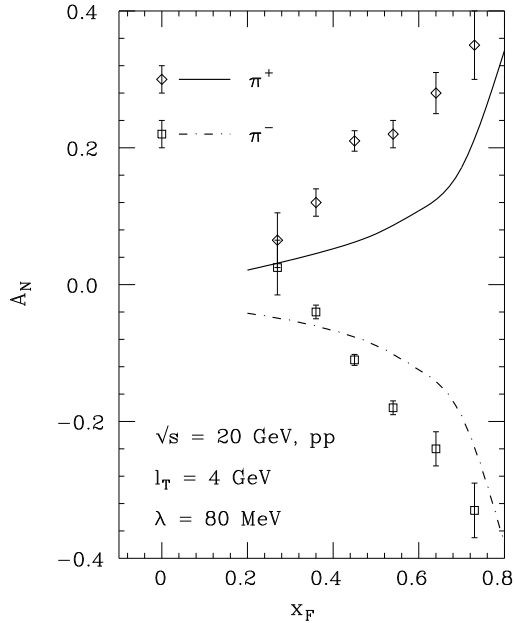


FIG. 21. Single transverse-spin asymmetry as a function of x_F for π^+ and π^- production with a polarized *proton* beam. Data are from Ref. [4]. Theory curves are evaluated at transverse momentum $l_T = 4$ GeV and with $\lambda = 0.080$ GeV.

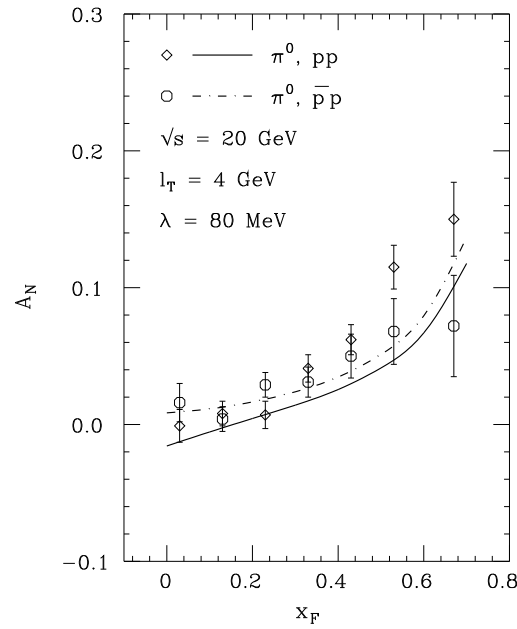


FIG. 22. Single transverse-spin asymmetry as a function of x_F for π^0 production with a polarized antiproton and proton beams. Data are from Ref. [4]. Theory curves are evaluated at transverse momentum $l_T = 4$ GeV and with $\lambda = 0.080$ GeV.

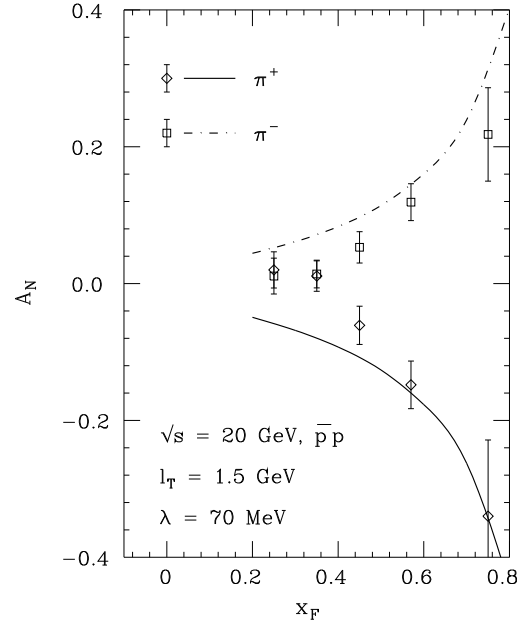


FIG. 23. Single transverse-spin asymmetry as a function of x_F for π^+ and π^- production with a polarized *antiproton* beam. Data are from Ref. [4]. Theory curves are evaluated at $l_T = 1.5$ GeV and $\lambda = 0.070$ GeV.

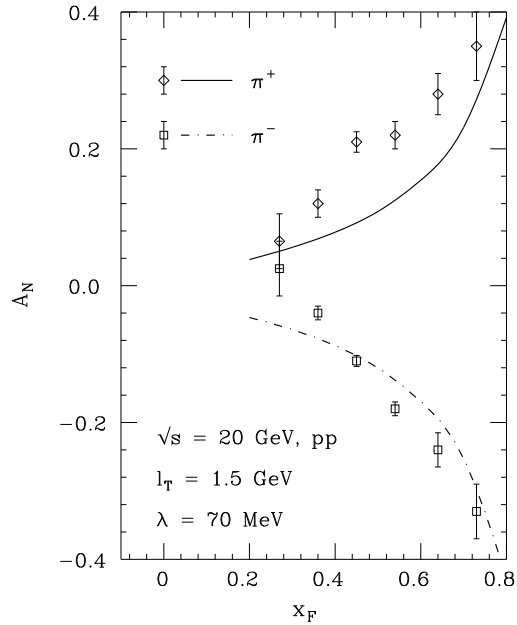


FIG. 24. Single transverse-spin asymmetry as a function of x_F for π^+ and π^- production with a polarized *proton* beam. Data are from Ref. [4]. Theory curves are evaluated at $p_T = 1.5$ GeV and $\lambda = 0.070$ GeV.

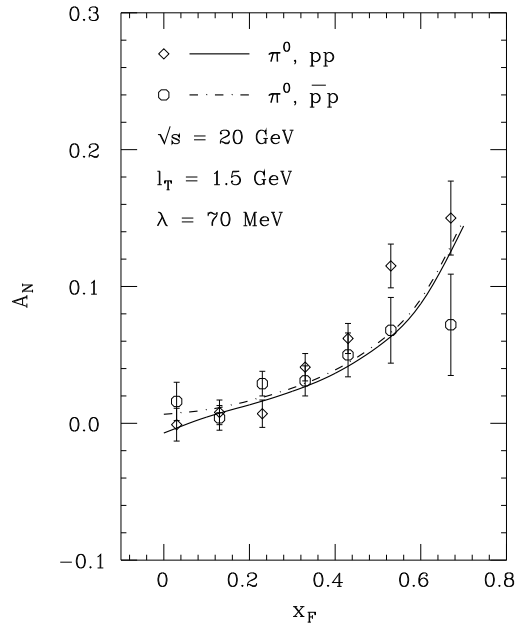


FIG. 25. Single transverse-spin asymmetry as a function of x_F for π^0 production with a polarized antiproton, along with the same asymmetry obtained with a polarized proton beam. Data are from Ref. [4]. Theory curves are evaluated at $l_T = 1.5$ GeV and $\lambda = 0.070$ GeV.

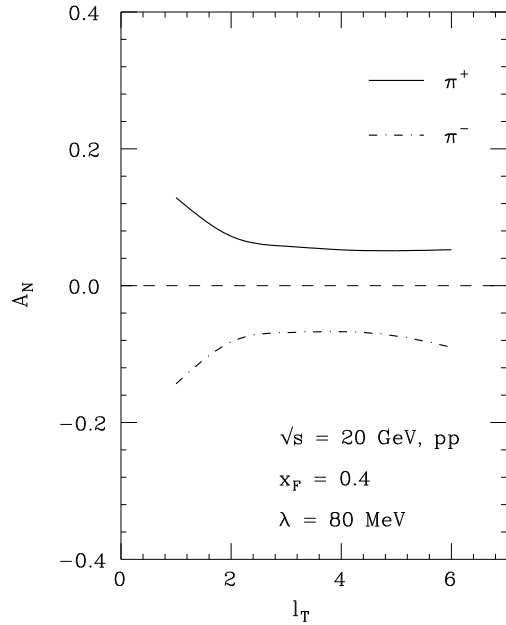


FIG. 26. Single transverse-spin asymmetry for π^+ and π^- production with a polarized *proton* beam as a function of pion's transverse momentum l_T . Theory curves are evaluated at $x_F = 0.4$, $\sqrt{S} = 20$ GeV and $\lambda = 0.080$ GeV.

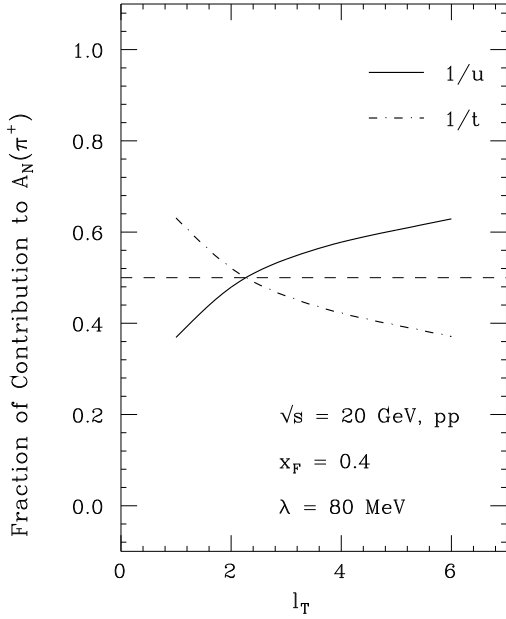


FIG. 27. Fractional contribution from $1/(-U)$ and $1/(-T)$ terms to the single transverse-spin asymmetry of π^+ production as a function of pion transverse momentum. Theory curves are evaluated at $x_F = 0.4$, $\sqrt{S} = 20$ GeV and $\lambda = 0.080$ GeV.

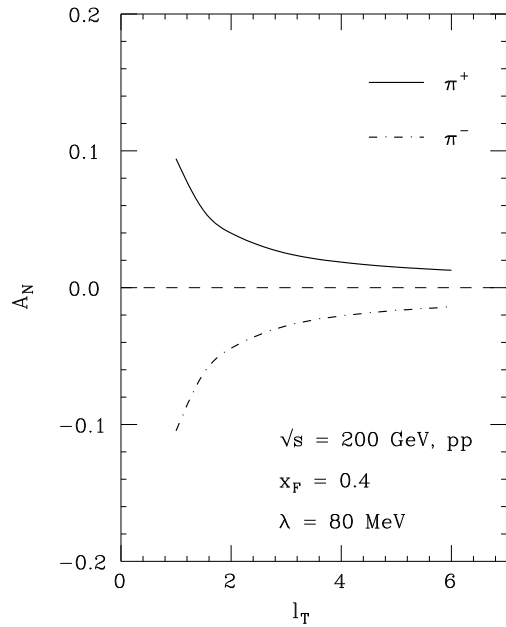


FIG. 28. Single transverse-spin asymmetry for π^+ , π^- and π^0 production with a polarized proton beam, as a function of pion transverse momentum l_T . Theory curves are evaluated at $x_F = 0.4$, $\sqrt{S} = 200$ GeV and $\lambda = 0.080$ GeV.

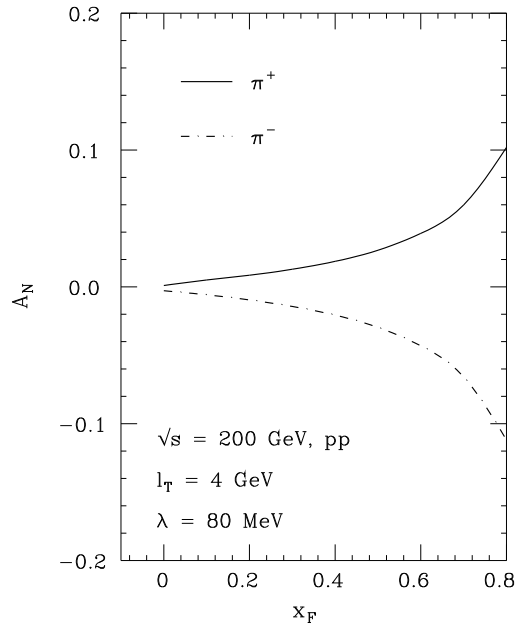


FIG. 29. Single transverse-spin asymmetry for π^+ , π^- and π^0 production with a polarized proton beam, as a function of pion transverse momentum l_T . Theory curves are evaluated at $x_F = 0.4$, $\sqrt{S} = 200$ GeV and $\lambda = 0.080$ GeV.

TABLES

TABLE I. Partonic hard parts and corresponding color factors for quark-gluon and anti-quark-gluon (indicated by barred letters) subprocesses. Feynman diagrams are shown in Fig. 15. C_g , C_g^I , and C_g^F are color factors for spin-averaged, spin-dependent with initial-state interaction, and spin-dependent with final-state interaction subprocess, respectively. The explicit factors (-1) are due to the sign difference between quark and antiquark propagators with the same momentum. Calculations were done in Feynman gauge.

Diagram	Partonic Parts		C_g	C_g^I	C_g^F
(a)	4	$1 - \frac{\hat{s}\hat{u}}{\hat{t}^2}$	$\frac{1}{2}$	$-\frac{N^2}{4(N^2-1)}$	$-\frac{1}{2(N^2-1)}$
(b)	2	$\frac{-\hat{u}}{\hat{s}}$	$\frac{N^2-1}{4N^2}$	$-\frac{1}{4}$	$\frac{1}{4N^2(N^2-1)}$
(c)	2	$\frac{\hat{s}}{-\hat{u}}$	$\frac{N^2-1}{4N^2}$	$\frac{1}{4(N^2-1)}$	$\frac{1}{4N^2(N^2-1)}$
(d)	$(+i)2$	$\frac{\hat{s}}{\hat{t}}$	$(-i)\frac{1}{4}$	$(+i)\frac{N^2}{4(N^2-1)}$	$(+i)\frac{1}{4(N^2-1)}$
(e)	$(-i)2$	$\frac{\hat{s}}{\hat{t}}$	$(+i)\frac{1}{4}$	$(-i)\frac{N^2}{4(N^2-1)}$	$(-i)\frac{1}{4(N^2-1)}$
(f)	$(-i)2$	$\frac{\hat{u}}{\hat{t}}$	$(+i)\frac{1}{4}$	0	$(-i)\frac{1}{4(N^2-1)}$
(g)	$(+i)2$	$\frac{\hat{u}}{\hat{t}}$	$(-i)\frac{1}{4}$	0	$(+i)\frac{1}{4(N^2-1)}$
(h)	0		—	—	—
(i)	0		—	—	—
(\bar{a})	4	$1 - \frac{\hat{s}\hat{u}}{\hat{t}^2}$	$\frac{1}{2}$	$\frac{N^2}{4(N^2-1)}$	$-\frac{1}{2(N^2-1)} (-1)$
(\bar{b})	2	$\frac{-\hat{u}}{\hat{s}}$	$\frac{N^2-1}{4N^2}$	$\frac{1}{4}$	$\frac{1}{4N^2(N^2-1)} (-1)$
(\bar{c})	2	$\frac{\hat{s}}{-\hat{u}}$	$\frac{N^2-1}{4N^2}$	$-\frac{1}{4(N^2-1)}$	$\frac{1}{4N^2(N^2-1)} (-1)$
(\bar{d})	$(-i)2$	$\frac{\hat{s}}{\hat{t}}$	$(+i)\frac{1}{4}$	$(+i)\frac{N^2}{4(N^2-1)}$	$(-i)\frac{1}{4(N^2-1)} (-1)$
(\bar{e})	$(+i)2$	$\frac{\hat{s}}{\hat{t}}$	$(-i)\frac{1}{4}$	$(-i)\frac{N^2}{4(N^2-1)}$	$(+i)\frac{1}{4(N^2-1)} (-1)$
(\bar{f})	$(+i)2$	$\frac{\hat{u}}{\hat{t}}$	$(-i)\frac{1}{4}$	0	$(+i)\frac{1}{4(N^2-1)} (-1)$
(\bar{g})	$(-i)2$	$\frac{\hat{u}}{\hat{t}}$	$(+i)\frac{1}{4}$	0	$(-i)\frac{1}{4(N^2-1)} (-1)$
(\bar{h})	0		—	—	—
(\bar{i})	0		—	—	—

TABLE II. Partonic hard parts and corresponding color factors for subprocesses involving quarks and/or antiquarks. Feynman diagrams are shown in Fig. 17. In diagrams (i) and (j) both fermion arrows have been reversed, relative to (i) and (j). C_q , C_q^I , and C_q^F are color factors for spin-averaged, spin-dependent with initial-state interaction, and spin-dependent with final-state interaction, respectively. Flavor indices a and b correspond to the flavor of the quark (or antiquark) from the polarized hadron and unpolarized hadron, respectively, and c is the flavor of fragmenting quark. The explicit factors (-1) are due to the sign difference between quark and antiquark propagators with the same momentum. Calculations were done in Feynman gauge.

Diagrams	Partonic Parts		C_q	C_q^I	C_q^F	
(a)	2	$\frac{\hat{s}^2 + \hat{u}^2}{\hat{t}^2}$	δ_{ac}	$\frac{N^2 - 1}{4N^2}$	$\frac{N^2 - 4N - 4}{32N}$	$-\frac{1}{4N^2}$
(b)	2	$\frac{\hat{s}^2 + \hat{u}^2}{\hat{t}^2}$	δ_{ac}	$\frac{N^2 - 1}{4N^2}$	$\frac{N^2 + 4N - 4}{32N} (-1)$	$-\frac{1}{4N^2}$
(c)	2	$\frac{\hat{s}^2 + \hat{u}^2}{\hat{t}^2}$	δ_{ac}	$\frac{N^2 - 1}{4N^2}$	$\frac{N^2 + 4N - 4}{32N}$	$-\frac{1}{4N^2} (-1)$
(d)	2	$\frac{\hat{s}^2 + \hat{u}^2}{\hat{t}^2}$	δ_{ac}	$\frac{N^2 - 1}{4N^2}$	$\frac{N^2 - 4N - 4}{32N} (-1)$	$-\frac{1}{4N^2} (-1)$
(e)	2	$\frac{\hat{s}^2 + \hat{t}^2}{\hat{u}^2}$	δ_{bc}	$\frac{N^2 - 1}{4N^2}$	$\frac{N^2 - 4N - 4}{32N}$	$\frac{N^2 + 4N - 4}{32N}$
(f)	2	$\frac{\hat{s}^2 + \hat{t}^2}{\hat{u}^2}$	δ_{bc}	$\frac{N^2 - 1}{4N^2}$	$\frac{N^2 + 4N - 4}{32N}$	$\frac{N^2 - 4N - 4}{32N}$
(g)	2	$\frac{\hat{s}^2 + \hat{t}^2}{\hat{u}^2}$	δ_{bc}	$\frac{N^2 - 1}{4N^2}$	$\frac{N^2 + 4N - 4}{32N} (-1)$	$\frac{N^2 - 4N - 4}{32N} (-1)$
(h)	2	$\frac{\hat{s}^2 + \hat{t}^2}{\hat{u}^2}$	δ_{bc}	$\frac{N^2 - 1}{4N^2}$	$\frac{N^2 - 4N - 4}{32N} (-1)$	$\frac{N^2 + 4N - 4}{32N} (-1)$
(i)	2	$\frac{\hat{s}^2}{\hat{t} \hat{u}}$	$\delta_{ab} \delta_{ac}$	$-\frac{N^2 - 1}{4N^3}$	$\frac{N^2 + 1}{4N^3}$	$\frac{1}{4N^3}$
(j)	2	$\frac{\hat{s}^2}{\hat{t} \hat{u}}$	$\delta_{ab} \delta_{bc}$	$-\frac{N^2 - 1}{4N^3}$	$\frac{N^2 + 1}{4N^3}$	$\frac{1}{4N^3}$
(ī)	2	$\frac{\hat{s}^2}{\hat{t} \hat{u}}$	$\delta_{ab} \delta_{ac}$	$-\frac{N^2 - 1}{4N^3}$	$\frac{N^2 + 1}{4N^3} (-1)$	$\frac{1}{4N^3} (-1)$
(j̄)	2	$\frac{\hat{s}^2}{\hat{t} \hat{u}}$	$\delta_{ab} \delta_{bc}$	$-\frac{N^2 - 1}{4N^3}$	$\frac{N^2 + 1}{4N^3} (-1)$	$\frac{1}{4N^3} (-1)$
(k)	2	$\frac{\hat{t}^2 + \hat{u}^2}{\hat{s}^2}$	$\delta_{a\bar{b}}$	$\frac{N^2 - 1}{4N^2}$	$-\frac{1}{4N^2} (-1)$	$\frac{N^2 + 4N - 4}{32N}$
(l)	2	$\frac{\hat{t}^2 + \hat{u}^2}{\hat{s}^2}$	$\delta_{a\bar{b}}$	$\frac{N^2 - 1}{4N^2}$	$-\frac{1}{4N^2}$	$\frac{N^2 - 4N - 4}{32N}$
(m)	2	$\frac{\hat{t}^2 + \hat{u}^2}{\hat{s}^2}$	$\delta_{a\bar{b}}$	$\frac{N^2 - 1}{4N^2}$	$-\frac{1}{4N^2} (-1)$	$\frac{N^2 - 4N - 4}{32N} (-1)$
(n)	2	$\frac{\hat{t}^2 + \hat{u}^2}{\hat{s}^2}$	$\delta_{a\bar{b}}$	$\frac{N^2 - 1}{4N^2}$	$-\frac{1}{4N^2}$	$\frac{N^2 + 4N - 4}{32N} (-1)$